Silanol defects engineering and healing in zeolites: Opportunities to fine-tune their properties and performances

Izabel C Medeiros-Costa, Eddy Dib, Nikolai Nesterenko, Jean-Pierre Dath, Jean-Pierre Gilson, Svetlana Mintova

ARTICLE

Silanol defects engineering and healing in zeolites: Opportunities to fine-tune their properties and performances

Received 00th January 20xx,
Accepted 00th January 20xx

DOI: 10.1039/x0xx00000x

Izabel C. Medeiros-Costa[a,b,#], Eddy Dib[a,#], Nikolai Nesterenko[b], Jean-Pierre Dath[b], Jean-Pierre Gilson[a], Svetlana Mintova[a,*]

Zeolites have been game-changing materials in oil refining and petrochemistry over the last 60 years and have the potential to play the same role in the emerging processes of the energy and environmental transition. Although zeolites are crystalline inorganic solids, their structures are not perfect and the presence of defects sites – mainly Brønsted acid sites and silanols - influences their thermal and chemical resistance as well as performances in key areas such as catalysis, gas and liquid separations and ion-exchange. In this paper, we review the type of defects in zeolites and the characterization techniques used for their identification and quantification with the focus on diffraction, spectroscopic and modeling approaches. More specifically, throughout the review, we will focus on silanol (Si-OH) defects located within the micropore structure and/or on the external surface of zeolites. The main approaches applied to engineer and heal defects and their consequences on the properties and applications of zeolites in catalysis and separation processes are highlighted. Finally, the challenges and opportunities of silanol defects engineering in tuning zeolites properties to meet the requirements for specific applications are presented.

1. Introduction

Zeolites are porous crystalline inorganic solids, formed by connecting tetrahedrally coordinated (T) atoms. They were initially defined as microporous aluminosilicate minerals but several elements have been steadily introduced in their framework by isomorphous substitution. Their T-O-T bonds (T = Si, Al…) form tetrahedra and these so-called primary building units further assemble as polyhedras (secondary building units) connecting to develop periodic three-dimensional microporous crystalline structures.[1,2] Theoretically, they could grow infinitely without imperfections, except for those at their external surface.

In this review, a defect is defined as a perturbation in the crystalline arrangement that will somehow break the perfect symmetry expected from the periodic association of TO_4 units. While a neutral network is ideally expected in pure silica zeolites, the presence of Al^{3+} in a Si^{4+} oxide (O^{2-}) network creates a negative charge on the framework necessarily balanced by an extra-framework positive charge. Brønsted acid sites (BAS), often referred to as bridged hydroxyls, are formed when the extra-framework positive charge is a proton bound to one of the oxygens in the Al tetrahedron [Si-O(H)-Al]. Such a "defect" is at the origin of the remarkable properties of zeolites in acid catalyzed reactions as these sites and the reactants are confined in a well-defined molecular-size environment.[3]

Silanols (Si-OH) are also structural defects in the internal structure or on the external surface of zeolites. The internal ones commonly result from unbalanced charges in the zeolitic framework, while the external silanols are needed to complete the valence of oxygen atoms once the crystal growth stops.[4] These silanols display a weaker acid strength than the BAS and are typically constituted of hydroxyl groups.[3,4] Thus, different types of silanol defects are commonly present in zeolites as outlined in Fig. 1.[4] Throughout the review, we will refer to them as silanol (Si-OH) defects, although they can appear in multiple forms in zeolites.

Isolated silanols are commonly observed at crystal terminations. Other defects resulting from missing one or more T-O-T bonds are also observed: geminal, vicinal, bridged silanols and also in clusters of the type [SiO^-...HOSi].[5,6] Their configurations can further vary slightly due to clustering as in silanol nests formed by the vacancy created by a missing T atom (top right corner of Fig. 1). The classic representation of silanol nests corresponds to the presence of four hydrogen-bonded Si-OH silanols due to their proximity. However, such a configuration does not appear to be stable enough and alternative configurations that consist of pairs or triad of ≡SiO^----HO-Si≡ species were considered.[6,7]

[a.] *Laboratoire Catalyse et Spectrochimie (LCS), Normandie University, ENSICAEN, CNRS, 6 boulevard du Marechal Juin, 14050 Caen, France.*
[b.] *Total Research and Technology Feluy, B-7181 Seneffe, Belgium.*
[#] *These authors contributed equally to this work*
**mintova@ensicaen.fr*

ARTICLE

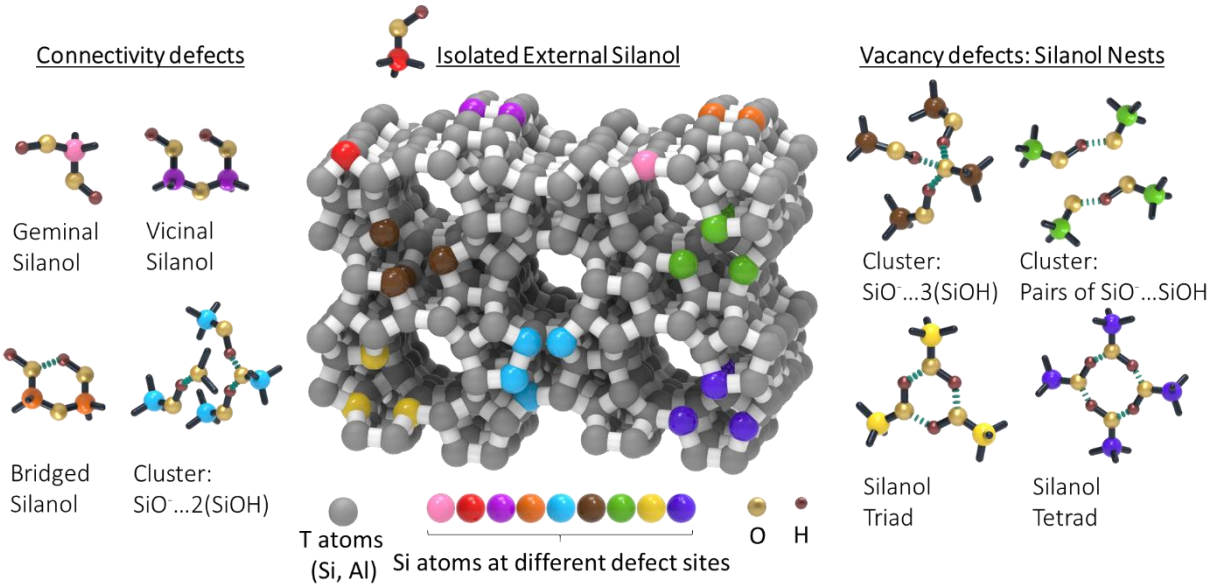

Fig. 1 *Schematic representation of different types of silanols grouped into three main categories: isolated external silanols, connectivity defects and vacancy defects. Green dotted lines indicate hydrogen bonding.*

Defects offer an alternative to compensate a charge imbalance in the zeolite structure. Their formation results from (i) different synthetic methodologies and the nature and purity of the reagents and (ii) post-synthesis treatments of zeolites. Legacy and new syntheses as well as post-synthesis strategies were developed to overcome the most nagging drawback of zeolites, *i.e.* the severe transport limitations (*e.g.* configurational diffusion) leading sometimes to the inaccessibility of bulky molecules to active sites in catalysis or adsorption. The resulting so-called hierarchical zeolites combining connected micro-, meso- and macro-porosities invariably possess defects to variable extents.

Recent research efforts focus on healing defects since they often adversely affect key zeolite properties like thermal and hydrothermal stability. This review will present the main approaches to engineer and heal defects including external heat treatments (calcination and steaming), alkali, transition metals and fluoride anions additions, *in-situ* and post-synthesis silylation, defects blocking with dye-based molecules, and selective coke deposition. Significant changes in the performance of zeolites in catalysis and adsorption are observed due to the presence of silanol defects. While the presence of silanols improves the catalytic performance of zeolites in specific reactions, some undesirable effects such as coke production and, consequently, shorter catalyst lifetime are also associated with the presence of defects. Adsorption of hydrophilic molecules is facilitated by the presence of defects while separation selectivity is more often lowered. In biomedical applications, the presence of silanols is key to a controlled release of drugs and the cell/zeolite adhesion.

An overview of the advances made in the characterization of defects in zeolites is presented. We focus on diffraction techniques (e.g., X-ray diffraction) as well as on spectroscopies (e.g., UV-Vis, Infrared and Nuclear Magnetic Resonance). They are the most used and contributed to a wealth of information on the identification, quantification and accessibility of Brønsted acid sites and silanols structural defects in zeolites. Theoretical modeling is also included as it provides added value to understand the experimental characterization results.

2. Detection of zeolite defects: main characterization approaches

As zeolitic O-H correspond to either Brønsted acid sites (BAS) or structural silanol defects, the characterization techniques of choice are mainly X-ray diffraction and spectroscopic techniques (UV-Vis, Fourier Transform Infrared (FTIR) and Nuclear Magnetic Resonance (NMR)). We briefly outline those used to identify, localize, and quantify defects as well as Density Functional Theory (DFT) calculations and refer the readers to in-depth reviews and their references.[8] They are as well as the information collected summarized in Table 1.

Table 1 Characterization techniques to probe defects in zeolites

Technique	Wave Energy (Hz)	Target	Information
X-ray Diffraction (XRD)	$10^{17} - 10^{20}$	Crystallographic planes	Lattice parameters, bond length, angles
Ultraviolet – Visible (UV-Vis)	$10^{15} - 10^{17}$	Valence Electrons	Coordination, oxidation state
Fourier Transform Infrared (FTIR)	$10^{13} - 10^{15}$	Dipolar Bonds	Bond vibration, acidity
Nuclear Magnetic Resonance (NMR)	$10^{6} - 10^{8}$	Nuclear spins	Local geometry, bonding, distances, dynamics

2.1. X-ray diffraction (XRD)

X-ray diffraction (XRD) exploits the interaction between X-rays (10^{17} – 10^{20} Hz), usually from *CuK*α, and crystal planes in a solid if any. Thus, crystalline materials are characterized by unique diffraction patterns providing structural information. This technique is still an affordable gold standard to solve zeolites structures. It is always the first method used (i) to determine the crystallinity of a zeolite, (ii) to identify the zeolite phase, (iii) to determine the unit cell parameters, (iv) to estimate the crystallites sizes and (v) to report the probable cationic sites.[9] We refer to the works of Breck et al. for zeolite LTA[10], Meier for MOR[11], Olson et al. for FAU[12], Koningsveld et al. for MFI[13], Baerlocher and McCusker for a large number of zeolites.[14] The crystal structures were solved either by single-crystal or by powder XRD techniques. However, the presence of pseudo-symmetry, intergrowth and disorder leading to peak overlapping make the structure resolution of powders less straightforward than for single crystals.[15] Thus, the use of Synchrotron X-ray diffraction increased, since it allows solving some complex structures.[16] Neutron and electron diffraction were also combined with XRD to increase resolution and sensitivity in zeolite structure determination.[17]

Knowing that (i) X-ray diffraction technique is based on the localization of electronic densities and (ii) aluminum (Al) and silicon (Si) have similar electronic densities, Al location in the framework is difficult to identify due to a lack of resolution especially for high Si containing materials.[18] The task is harder for Brønsted acid sites (BAS) and silanols, as the small size of hydrogen atom implies a low sensitivity. Defects location by XRD is therefore not straightforward. Several attempts to localize Al atoms by exchanging the protons with big cations were reported[19]. Pinar et al.[20] recently showed that Al location in FER zeolite can be probed by their organic structure directing agents. Lo et al. and Ye at al. also showed the location of BAS in the cross-channel region in H-ZSM-5[21] and H-USY[22] using pyridine as a probe molecule. Ordered silanols originating from silicon vacancies were found in SSZ-70 and SSZ-74 as well as in TNU-9 and IM-5 zeolites[23,24] (***Fig. 2***).

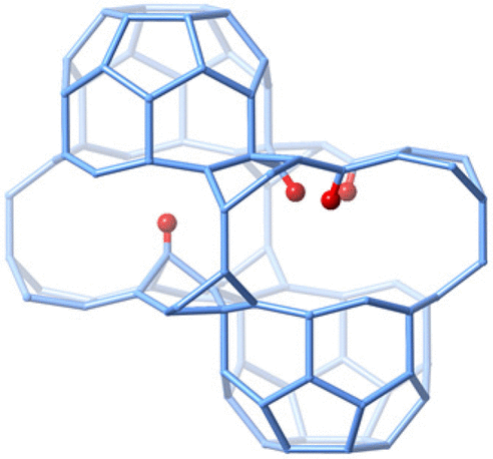

Fig. 2 *Ordered silicon vacancies in the framework structure of the zeolite catalyst SSZ-70 containing isolated –SiOH group and a nest of three Si–O–H groups in place of the three Si–O–Si linkages. This figure has been reproduced from ref 24 with permission from American Chemical Society, copyright 2017.*

2.2. Fourier Transform Infrared (FTIR) Spectroscopy

Infrared is a vibrational spectroscopy based on the interaction between an electromagnetic radiation (10^{13} and 10^{15} Hz) and species with a permanent or induced dipole. This technique was extensively used to probe the insertion and location of heteroatoms in zeolite frameworks, their acidity and guest–host interactions. The high potential of FTIR was demonstrated by the routine use of various probe molecules as CO, NO, Pyridine and many others[25]. Insightful correlations were established between the stretching frequencies and the Si-O and O-H distances.[26] However, the relation between Si/Al ratio, acidic strength and the stretching frequency of O-H groups was not straightforward.

The stretching vibrations of OH groups lie in the IR spectral region 3000 - 4000 cm^{-1} and their position depends on acid strength, confinement and location in the zeolite framework (Fig. 3). External and internal silanols positions overlap somewhat in the spectral region. As the characteristic stretching frequency of an OH group decreases with an

increase in hydrogen bonding,[27] isolated silanols appear around 3745 cm^{-1} while silanols with weak hydrogen bonds, such as vicinal silanols (3740 - 3730 cm^{-1}), internal silanols (3720-3710 cm^{-1}) are clearly distinguishable. Hydroxyls in Brønsted acid sites appear between 3650 and 3600 cm^{-1}. In the case of silanol nests, where the hydrogen bonds are the strongest, IR vibrations appear around 3500 cm^{-1}.

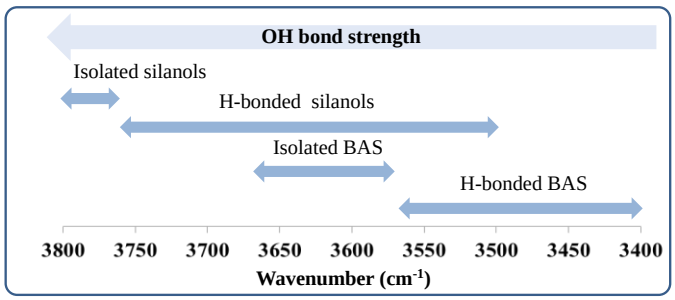

Fig. 3 *Characteristic stretching frequency of OH bonds in zeolites*

The quantification of silanols by IR uses the Beer-Lambert law. The molar absorption coefficient was derived from the correlation between the concentration of OH species and the area of the associated band. Although different silanols can be distinguished between 3745 and 3500 cm^{-1}, this spectral window is not the most convenient for quantification, since the presence of hydrogen bonding produces overlapping and can disturb the signal.[28] As an alternative, bands in the 4200-4800 cm^{-1} range could be used for quantification. A home-made technique, AGIR, namely the simultaneous recording of IR spectra and weight gain/loss by thermogravimetry (TG) allowed a very precise determination of the silanols molar absorption coefficient. The area of the bands in the 4200-4800 cm^{-1} range together with the water loss at different temperatures due to the condensation of silanols allowed an easy quantification of the total silanols but not to distinguish the different types.

The silanols accessibility could be quantified by exchange with deuterium oxide (D_2O) as the resulting Si-OD appear in the 2760-2700 cm^{-1} range. The deuteration of alcohols of various sizes by Si-OD groups highlighted the accessibility of Si-OH as a function of their confinement.[28]

2.3. Nuclear Magnetic Resonance (NMR) Spectroscopy

Solid-state Nuclear Magnetic Resonance (NMR) exploits the interaction between atomic active nuclei (Spin ≠ 0) and magnetic fields in the 10^6 – 10^8 Hz radiofrequency window. This technique provided precious structural and dynamic information in the last decades for zeolites thanks to the anisotropic – orientation dependent – interactions.[29] Although these interactions can be suppressed by the Magic Angle Spinning (MAS) technique or by Multiple-pluses sequences, the information present in the broadness of the spectra may be recovered using recoupling techniques (*vide infra*).

The four main internal nuclear spins interactions used to extract useful information are (i) the chemical shielding representing the interaction of a spin with the surrounding electrons, (ii) the quadrupolar coupling – only for nuclei having a quadrupolar moment (I > ½) – representing the interaction of a spin with the surrounding electric field gradient (EFG), (iii) the direct spin-spin coupling (dipolar coupling through the space) and (iv) the indirect spin-spin coupling (scalar coupling through the bonds). The relative intensity of each interaction and the related information are presented in Table 2.

Table 2 *Wavelengths and information extracted from the four main interactions exploited by solid-state NMR spectroscopy in zeolites.*

Interaction	Intensity (Hz)	Information
Quadrupolar	$0 – 10^7$	Local geometry
Dipolar	$0 – 5.10^4$	Distance
Shielding	$0 – 2.10^4$	Coordination, bond angle
Scalar	$0 – 10^2$	Chemical bonding

Being anisotropic, they are described by second rank Cartesian tensors characterizing their amplitude and symmetry. The related equations are well developed, and detailed information is available in the literature.[30]

In zeolites and related porous materials, the NMR active nuclei are numerous and include ^{29}Si, ^{27}Al, ^{17}O, ^{14}N, ^{1}H, ^{2}D; their potential is described below as they are related to Brønsted Acid Sites (BAS) or silanol defects.

Silicon-29 (I = 1/2, 4.700 % Natural Abundant) is the most reported nucleus in zeolites since Si is the main tetrahedral (T) atom in the framework, despite a low sensitivity due to its low natural abundance. In a landmark work, Engelhardt et al[31] showed that the ^{29}Si isotropic chemical shift is a function of the nature and the number of T neighbors. The ^{29}Si isotropic chemical shift increased following the trend : Si (4Si), Si (3Si, 1T), Si (2Si, 2T), Si (1Si, 3T), and Si (4T) (Fig. 4). The Q^n building units were defined as $SiO_{4-n}(OT)_n$ units. Linear correlations were established between the isotropic chemical shift and the Si-O-T angles, Si-Si distances and Si-O bond lengths. The framework Si/Al ratio can also be computed from a one-dimensional ^{29}Si NMR spectrum using the equation

$$(Si/Al = \sum_{n=0}^{4} I_{Si(nAl)} / \sum_{n=0}^{4} (\frac{n}{4}) I_{Si(nAl)}).$$

However when silanol defects are present, the resolution decreased and an overlap of silanols and BAS peaks occurred due to T-O-T angular distributions[30]. The Si/Al ratio is therefore often underestimated due to the contribution of silanol defects. However, assuming that peaks initially assigned to Si (1Al) and Si (2Al) contain a contribution of Si(OH) and $Si(OH)_2$ species, respectively, the total amount of silanols [Si(OH) + $Si(OH)_2$] may be estimated.

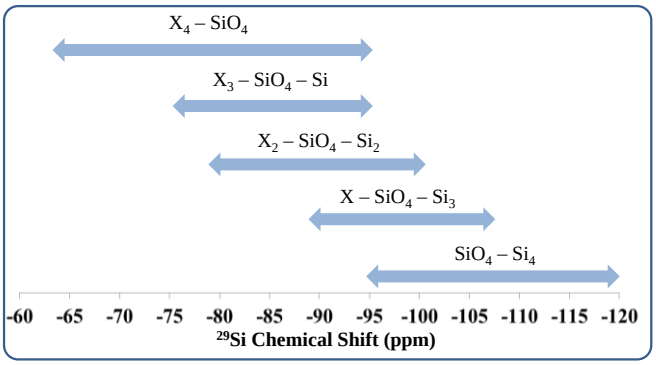

Fig. 4. *Characteristic ^{29}Si chemical shifts in zeolites*

Aluminium-27 (I = 5/2, 100 % Natural Abundant) is also a nucleus of interest since it generates Brønsted acid sites in zeolite frameworks. Tetra-coordinated Al (~60 ppm) in the framework and hexa-coordinated Al (~0 ppm) in extra-framework (EFAl) positions are easily distinguishable. Lipmaa et al. found several correlations between the chemical shift and the Al-O distances, Al-O-Al angles etc.[32] However, Al is a half integer nucleus interacting through its magnetic dipole moment with its surrounding electrons (chemical shielding) and through its electric quadrupolar moment with the Electric Field Gradient (EFG). This is a real advantage as its central transition peak contains much information but a band overlapping may occur. MQMAS pulse sequence introduced in 1995[33] permitted to obtain the highest resolution of the Al spectra and several attempts were made to localize the BAS using this sequence.[34,35] TRAPDOR pulse sequence was also used to probe the Al sitting in zeolites. Koller et al. used it recently to determine the ^{1}H–^{27}Al proximities in ZSM-5 with different Si/Al ratios to localize the BAS and assign the ^{1}H NMR peaks to either BAS or silanols.[36,37] Recently, tri-coordinated invisible Al species were identified in zeolites using trimethylphosphine oxide (TMPO) as probe molecules.[38]

Oxygen-17 (I = 5/2, 0.037 % Natural Abundant) is a key atom in zeolites. The primary TO_4 units are connected by sharing an oxygen and it is the main atom that handles BAS and silanols defects. However, the number of reports dealing with the oxygen nucleus remains low because of two factors: (i) the low natural abundance and the need of enrichment and (ii) the peak overlapping due to angular distributions and different crystallographic positions. BAS were detected with ^{17}O NMR in FAU zeolites.[39,40] Ashbrook et al. also used ^{17}O NMR to probe BAS in a wide variety of zeolites (
Fig. ***5***).[41,42] Pruski et al. distinguished between isolated and vicinal silanols using natural abundant ^{17}O NMR combined with Dynamic Nuclear Polarization probing selectively the surface.[43]

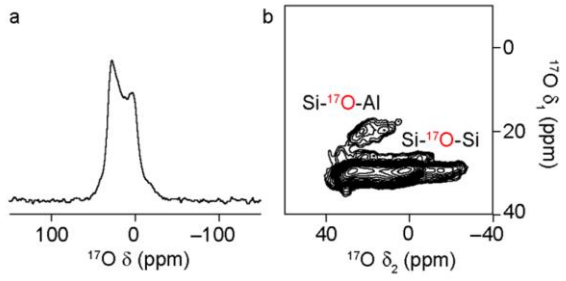

Fig. 5 *(a) MAS and (b) MQMAS spectra of ^{17}O enriched H-MOR zeolites. This figure has been reproduced from ref 42 with permission from American Chemical Society, copyright 2020.*

Nitrogen-14 (I = 1, 99.632 % Natural Abundant) was used to determine the Al or silanol location in as-synthesized zeolites in the presence of organic structure directing agents. However, it is an integer spin nucleus giving wide spectra because of the absence of a central transition like in ^{27}Al and ^{17}O. A statistical distribution of quadrupolar coupling parameters was observed due to the distribution on several sites of silanol defects in the framework of silicalite-1 and Al in ZSM-5. However, it is a very sensitive nucleus to monitor the degree of order in zeolite frameworks,

Fig. 6. The spectra may be modeled to quantify the order/disorder in zeolite frameworks, as in the case of silicalite-1 synthesized in the fluoride medium.[44,45]

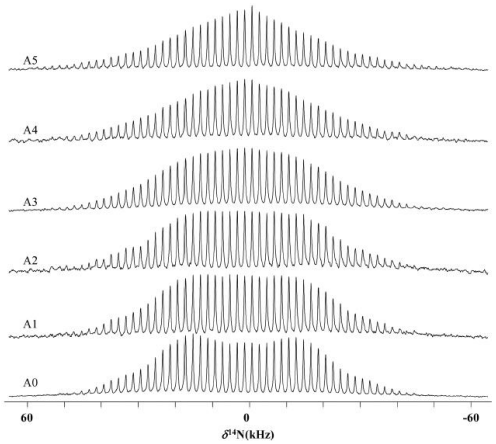

Fig. 6 *Evolution of the ^{14}N spectra with the aluminium loading in a series of as-synthesized ZSM-5 zeolites. This figure has been reproduced from ref 45 with permission from American Chemical Society, copyright 2017.*

Proton-1 (I = 1/2, 99.984 % Natural Abundant) is by far the most abundant and sensitive nucleus in NMR. Depending on the chemical shifts one can identify different hydroxyl species: isolated, internal, bridging (SiOHAl) and H-bonded silanols. The low resolution in the ^{1}H spectra and overlapping peaks render quantification and assignment difficult in a narrow 5 ppm chemical shift range.[46,47]

Proton NMR is obviously advantageous when the protons concentration is low. However, with a high proton concentration, strong dipolar couplings occurred as they are related to the inter-nuclear distance and collecting well-resolved ^{1}H NMR spectra is therefore not possible. Magic angle spinning (MAS) and several homo-nuclear decoupling sequences were developed in the last decades to mitigate the problem but by enhancing the resolution of the ^{1}H NMR spectra precious structural and dynamical information are lost. The so-called recoupling techniques were developed to reintroduce anisotropic interactions. Among them, the most valuable is the Multiple-Quantum–Single-Quantum (MQ-SQ) correlation methods restoring through-space dipole-dipole coupling while preserving the high spectral resolution provided by fast MAS spinning.

Dib et al. recently used ^{1}H double-quantum single-quantum (DQ-SQ) MAS NMR to locate silanol defects in silicalite-1 synthesized with different templates.[48,49] Koller et al. expanded the study to other zeolites including ZSM-12, ZSM-5, SSZ-24 and SSZ-74. Structural defects location is therefore governed by the Organic Structure Directing Agent (OSDA) used (
Fig. ***7***).[6]

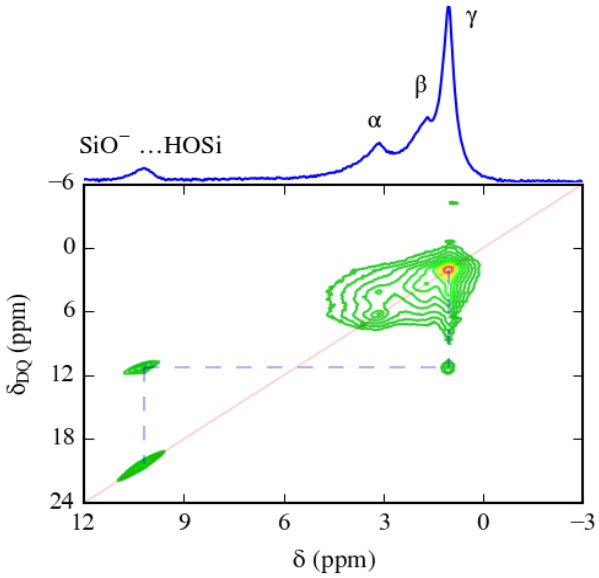

Fig. 7 *DQ-SQ ^{1}H NMR spectrum showing the interaction between an OSDA and the structural silanols in as-synthesized silicalite-1. This figure has been reproduced from ref 48 with permission from American Chemical Society, copyright 2015.*

Silanol triads were found in calcined SSZ-70[7] and other zeolites together with hydrogen-bonded silanols and BAS using ^{1}H double-quantum single-quantum (DQ-SQ) MAS NMR correlation and ^{1}H{^{27}Al} rotational echo adiabatic pulse double resonance (REAPDOR) spectroscopy.[36]

Deuterium-2 (I = 1, 0.011% Natural Abundant) is the second isotope of hydrogen and less studied in NMR because of its low natural abundance and its quadrupolar moment. However, when enriched with deuterium, Brønsted acid sites and silanols in RHO[50] and FAU[51,52] zeolites have distinct spectral features related to their framework location. ^{2}D NMR efficiently probed the dynamics of organic molecules,[53] and X and Y zeolites loaded with deuterated water at different temperatures contributed to the analysis of the peaks corresponding to BAS and silanols.[54] Moreover, important information on the confinement of water molecules in zeolites cages can be collected. A recent theoretical study showed the high sensitivity of deuterium quadrupolar coupling parameter towards the O-D distance.[55]

2.4. UV-Vis

UV-Vis is an electronic spectroscopy that exploits the interaction of a UV radiation in the of 10^{15} – 10^{17} Hz window. This technique was mainly used to characterize Titanium (Ti) coordination in TS-1 zeolites.[56] Dedececk et al. characterized BAS in several zeolites by UV-Vis[57] and highlighted Al locations in various framework sites, like rings, channels or cavities and their distribution between isolated and close Al in various Al-O-(Si-O)$_n$-Al sequences. Close Al – facing the same channel – attracted cobalt hexaquo-complex $[Co^{2+}(H_2O)_6]^{2+}$ at the expense of the more isolated Al. In turn, the zeolite exchange capacity for this divalent complex was a likely indicator of close Al atoms in the zeolite structure.[58]

2.5. Modelling

In the last decade, “NMR crystallography” emerged in the field of zeolites.[59–62] It combines structural and crystallographic information to refine a complex structure or validate a structural model using NMR data. Zeolites were among the first candidates selected, using the NMR-derived local order information with the diffraction-derived long-range order. Computational methods, e.g., density functional theory (DFT), were often used in cluster or periodic approaches and the results used as restraints to further refine structural models or eliminate mismatches. This methodology was recently used by Alonso et al. to locate Al atoms in specific sites in as synthesized ZSM-5. By combining Dipolar-Heteronuclear Multiple Quantum Correlation (D-HMQC) between ^{29}Si – ^{27}Al NMR and quantum chemistry calculations they reported the Al siting in as synthesized ZSM-5 in fluoride media; this material contains a very small amount of silanol defects as shown in

Fig. 8.[63]

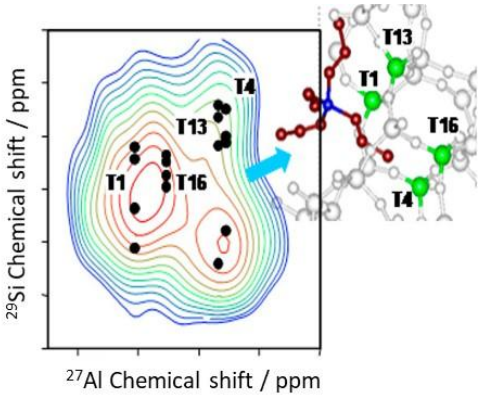

Fig. 8 *Correlation between computed Si and Al chemical shifts (ppm) and D-HMQC 2D NMR spectrum. [Reproduced with permission] This figure has been reproduced from ref 63 with permission from American Chemical Society, copyright 2018.*

The combination of FTIR and theoretical calculations also permitted to locate BAS.[64,65] Chizalet et al., combined ^{1}H NMR and IR with DFT, and proposed several types of silanols and BAS sites in ZSM-5.[66] Koller et al. suggested different BAS in a series of zeolites based on specific angles and orientation needed to be Hydrogen bonded.[37]

3. Engineering defects in zeolites

The presence of defects in zeolites is related to the synthesis and post-synthesis treatment methods applied. The strategies explored to engineer defects in zeolites will be discussed as depicted in Fig. 9: (1) synthesis of layered zeolite structures, (2) generation of mesopores, (3) creation of defects by water intrusion and (4) formation of defects by crystal size reduction.

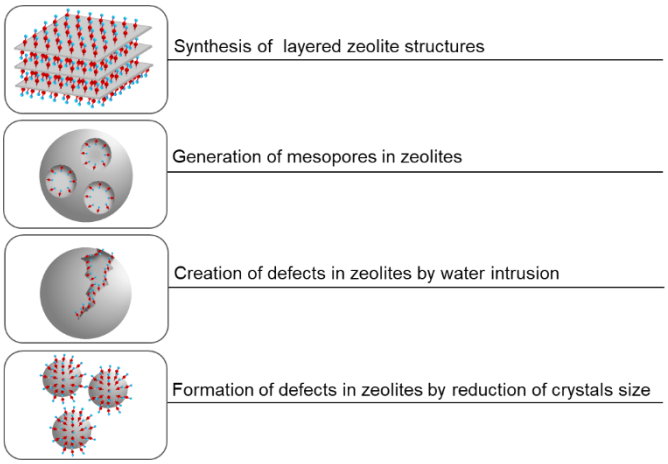

Fig. 9 *Overview of strategies to engineer defects in zeolites.*

3.1. Synthesis of layered zeolite structures

Silanol defects are intrinsically present at the termination of zeolite crystals. Layered zeolites contained significant amounts of such defects due to their high surface to bulk ratio. The layered zeolitic precursor with MWW structure was among the first to be delaminated, producing zeolite ITQ-2.[67] The stacking of the layered precursor was broken, separating the layers and forming a highly accessible house of cards structure. The ITQ-2 layers are rich in terminal silanols (**Erreur ! Source du renvoi introuvable.**) as indicated by a peak at -102 ppm in their ^{29}Si NMR spectra.[67]

Other post-synthesis modifications of layered MWW precursors to maximize accessibility of their active sites were reported (**Erreur ! Source du renvoi introuvable.**).[68,69] MCM-36 was formed by pillaring a MWW precursor with silica pillars.[70] The silanols were located on the silica pillars and at the remaining external surface of the zeolitic layers.[71] Expansion by insertion of silicon bridges (O-Si-O) between two zeolitic layers also generated new silanols. In this case, geminal silanols (Q_2) were formed by eliminating the methyl groups of the silane forming the silicon bridges.[72] Some of the original silanols were healed due to their interactions with the silane.[72] MCM-56 was another material made of exfoliated MWW layers. In this case, no post treatment was needed as layer exfoliation results from the intercalation of organic cations (tetraethylammouniums) between adjacent MWW layers.[73] MCM-56 was therefore a disordered delaminated and highly defective structure, due to the presence of silanols on the layers and possesses more Q^3 species than the tri-dimensional MCM-49 (
Fig. ***11***).[37,74]

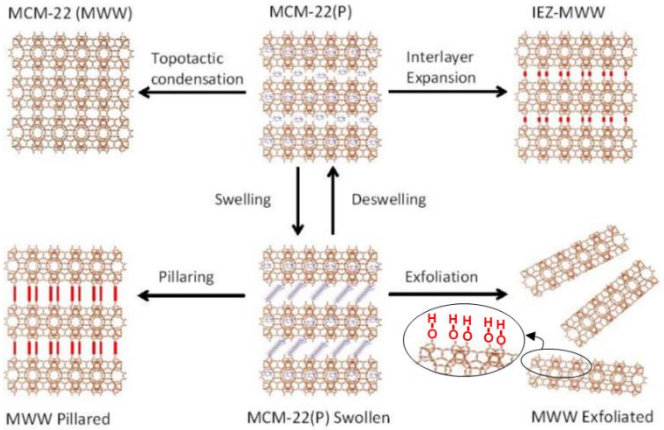

Fig. 10 *Schematic representation of the layered MWW precursor (MCM-22 P) and derived structures obtained through different post-synthesis treatments. This figure has been adapted from ref 69 with permission from John Wiley and Sons, copyright 2014.*

MIT-1 was produced from MWW nanosheets using a bifunctional surfactant (Ada-i-16) in a one-pot synthesis.[75] It was very similar to the exfoliated ITQ-2 and MCM-56 and its high external surface area suggested the presence of a substantial amount of silanols. The selective titration of the external surface sites by tributylphosphine oxide (TBPO) monitored by ^{31}P MAS NMR indicated that the MIT-1 had three times more sites than the MCM-22, a 3D zeolite with a lower external surface.[75]

Fig. 11 *^{29}Si NMR spectra of MCM-56 and MCM-49 zeolites highlighting Q_3 and Q_4 species associated with the silanol defects. This figure has been reproduced from ref 73 with permission from Elsevier, copyright 2020.*

Other zeolites like MFI were also synthesized as nanosheets with large external surfaces.[76–79] Single-unit-cell MFI nanosheets, synthesized in the presence di-quaternary ammonium-type surfactant, possess a significantly higher BET surface area compared to conventional MFI, a material likely to have many defects.[79] The presence of defects in the MFI nanosheets synthesized using a mixture of tetrapropylammonium hydroxide (TPAOH) and a polyquaternary ammonium surfactant (referred to as C22) was assessed by ^{29}Si MAS and {^{1}H} ^{29}Si CP NMR.[77] All zeolites contained silanols, as evidenced by their Q_3 signal in the ^{29}Si NMR spectra. {1H} ^{29}Si CP NMR indicated a reduction of Q^2 species for the zeolite synthesized with the highest TPAOH concentration (10/12 C22/TPAOH ratio).[77] The reduction of its Q^2 signal intensity seemed associated with its lower mesoporous volume and external surface area.

MEL/MFI intergrowths were also used to produce single unit cell layers of pure silica zeolites, SPP (Self-Pillared Pentasil), where two organic templates (tetrabutylphosphonium and tetrabutylammonium hydroxides) promoted intergrowths.[78] SPP occurred as MEL phase grew on pre-existing MFI nanosheets, the former linking the latter. These 2 nm tick SPP nanosheets possessed 2-7 nm mesopores.[78] Although no silanols characterization was reported, they should be present on this material as well. It is further expected that symmetry breaks at the edges of the MFI nanosheets and would contribute to the formation of structural defects, different from those silanols on the external surface.

Nanosheets were also produced as a result of FAU/EMT intergrowths.[80–82] The propagation of the intergrowths formed a cuboctahedra made of nanosheets interpenetrations at 70.5° and 109.5° angles (Fig. 12(a)).[81] As the EMT in (111) and $(11\bar{1})$ planes cannot be perfectly connected at 70.5°, the presence of defects at these intersections was expected. A schematic representation of such a structure is presented in Fig. 12 (b), although they have not been characterized in detail.[81]

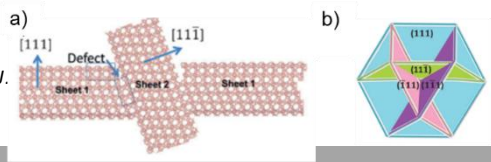

Fig. 12 *(a) Schematic representation of the branching mechanism leading to FAU/EMT intergrowth showing interpenetrating [111] and $[11\bar{1}]$ sheets and possible defects location. (b) Cuboctahedral skeletal base for the final structure presenting interpenetration at 70.5° and 109.5° angles. This figure has been reproduced from ref 81 with permission from John Wiley and Sons, copyright 2014.*

3.2. Generation of mesopores

The addition of mesoporosity to the native zeolite microporosity also produced defects in zeolites. The organic directing agent 3-(trimethoxysilyl)propyl] hexadecyldimethylammonium chloride used to synthesize MFI zeolite generated 3-8 nm mesopores.[83] Lee et al.[84], functionalized a parent MFI zeolite and its hierarchical

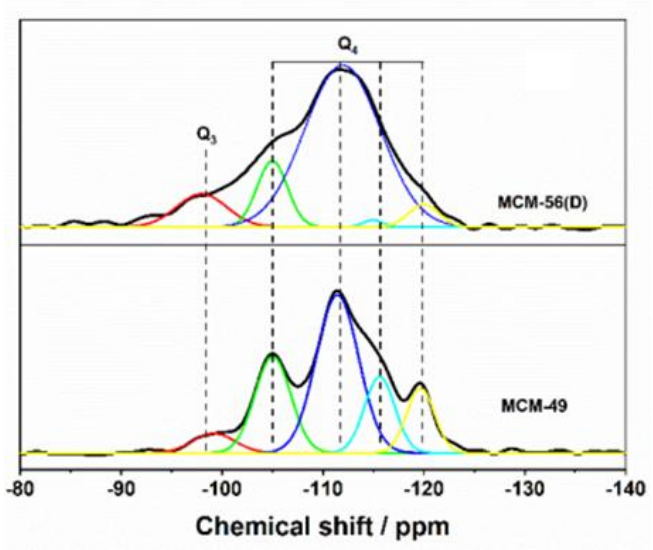

derivatives with alkoxysilanes, and reported higher functionalization on the latter zeolite due to a significantly higher amount of silanols. The silanol density of the hierarchical MFI zeolite was about twice higher than that of mesoporous SBA-15. Still regarding the MFI synthesis, using low temperature (100°C) and well-defined Si/Al (198), the propagation of defects was favored.[85] These defects in turn create intracrystalline mesopores, an attractive alternative to produce low-cost and environmentally friendly hierarchical zeolites.

The mordenite (MOR) zeolite synthesis was also modified by the addition of dual organic structure directing agents containing cetyltrimetylammonium and tetrapropylamonium ions to generate mesoporosity.[86] It is already known, by HREM and selected area electron diffraction, that the MOR structure contains several structural defects as dislocations, faults and intergrowth with dachiardite.[87] The disturbance generated by the organic templates during crystallization and a two-stage temperature treatment promoted the propagation of such defects and the creation of intracrystalline mesopores.[86] Polyacrylamide (PAM) and *n*-butylamine molecules were also used to produce mesoporous MOR zeolite.[88] An interesting effect is the increased Al incorporation in the MOR structure

by the addition of both templates as observed by ^{29} Si NMR and temperature programmed NH_3 desorption.[88] In addition, in the OH region of their IR spectra, a signal at 3734 cm^{-1} indicated the presence of silanols on the outer surface. Two other signals at 3606 cm^{-1} and 3545 cm^{-1} were identified as BAS located in the 8MR side-pockets and the 12MR channels, respectively. The contribution of BAS and silanols on the external surface was greater for the samples synthesized in the presence of templates.[88]

The use of charged organic structure directing agents (OSDA) is one of best-known factors responsible for the occurrence of defects in zeolites. Hunger et al.[89] proposed a model where Si-O^- species compensate the ionic charge of OSDA in as-synthesized zeolites. They stated that the presence of a Si-O^- group requires another analogous neighboring group, whose oxygen must be linked to an inorganic cation (such as Na^+), initially present in the reaction media (Fig. 13). ^{29}Si NMR spectroscopy showed that after Na^+ exchanged by a proton, new non-acid silanols (Si-OH) appeared and their concentration doubled compared to the calcined zeolite.

Fig. 13 *Role of tertaproplyammonium (TPA+) used as an organic structural directing agent (OSDA) on the formation of silanols in zeolites.*

Other treatments to generate mesopores based on a biased demetallation of the framework by caustic (preferential desilication) and acid (dealumination) leaching also produced defects. In the last decade, desilication by alkaline etching has been rediscovered and widely studied, in particular on MFI type zeolite.[90–94] Si and Al were removed from framework positions, but as silicate species are more soluble than aluminate species, the net result was an extensive desilication of the framework and a far more limited dealumination. Moreover, the Al dislodged from the framework was mostly retained on the zeolite and produced Lewis acidity; an optional acid treatment was necessary to remove this extra-framework Al, often detrimental in some 1D zeolites (TON, MTW…) as it blocked the native microporosity.[95,96] Its impact was best investigated by IR in the OH region.[92] After desilication, silanol nests (3490 cm^{-1}) disappeared in the parent MFI while the population of isolated silanols (3740 cm^{-1}) increased. This suggests that desilication started at the crystal boundaries and/or at silanol nests and further propagated to create mesoporosity where isolated silanols were required to terminate the crystals. Other hypotheses also suggested that the disappearance of silanol nests may be related to metal healing with Al atoms that could be eventually available.[92]

Acid leaching of zeolites is also a biased demetallation, *i.e.* Al was selectively removed from the framework and mostly washed away therefore increasing the overall and framework Si/Al ratios of the materials.[97–99] After dealumination of ZSM-5 with HCl, silanols were formed and observed by ^{29}Si NMR. This allowed, for instance, a subsequent inclusion of Ti in the framework.[99]

Steaming is also widely used for dealumination. This procedure has been industrially applied in the production of ultra-stable zeolite Y (USY) for decades,[100] widely used in FCC and hydrocracking of heavy crude fractions (atmospheric and vacuum gas oils or residues). It is also used for dealumination of ZSM-5 zeolite.[101,102] An increase in external silanols was observed as a function of steaming time [101] while the number of Brønsted acid sites decreased. In addition, a slight increase in silanol nests was observed by ^{1}H NMR; the spectra contain a peak at 2.5 +/-0.4 ppm as shown in red in Fig. 14. This suggests that the structure reorganized rapidly to heal these defects.[101]

Fig. 14 *^{1}H NMR spectra of ZSM-5 after steaming at different time intervals. This figure has been reproduced from ref 101 with permission from Elsevier, copyright 2012.*

A related method to dealuminate ZSM-5 was performed under

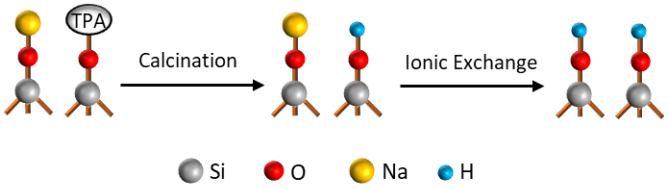

hot water treatment between 250 °C and 450 °C.[103] The behavior was similar to steaming and the silanols formation was observed (Fig. 15). The proposed mechanism indicated that the changes start to be observed at the external surface of the crystals, followed by Al-O bonds hydrolysis and subsequent deposition of extra-framework Al (EFAl). The

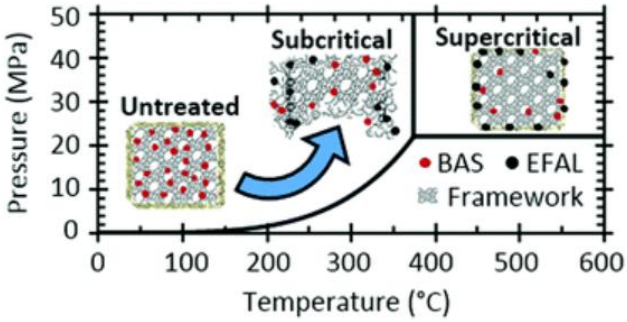

modifications undergone by the zeolites followed by infrared spectroscopic analysis indicated a reduction of Brønsted sites with an increasing temperature of treatment while the EFAl increased. Importantly, the (non-acid) silanols were not impacted by such hot water treatment. This may indicate that silanol nests, created by the Al removal, were rapidly healed by available and mobile Si atoms[103] in the steam treatment of zeolites.[101]

Fig. 15 *Effect of hot water treatment on silanol formation in zeolites. This figure has been reproduced from ref 103 with permission from Royal Society of Chemistry, copyright 2019.*

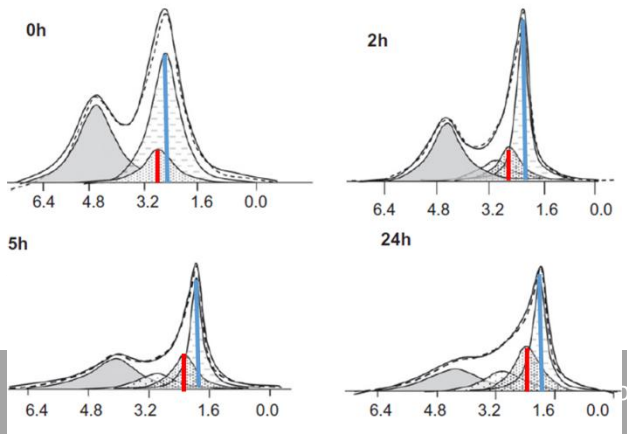

An interesting strategy to create mesopores with tunable dimensions in Y zeolite was proposed by Garcia - Martinez et al.[104] The method consisted of a partial dissolution of the zeolite in an alkali media and its recrystallization around surfactant micelles leading to the creation of well-defined mesopores. For high aluminum content zeolites, a dealumination step by acid washing had to be included prior to treatment with the surfactant. As defects were expected to appear during such treatments, their fate during different stages of the treatment was monitored by infrared spectroscopy in the OH region (3000 - 4000 cm^{-1}), Fig. 16. An important reduction of bridging hydroxyls was first observed as Al was removed during acid washing, and terminal silanols (3740 cm^{-1}) appeared on the external surface of the zeolite (Fig. 16 (b)). Their concentration increasing after treatment with the surfactant (Fig. 16 (c)), was indicative of the presence of the mesopores. However, after heat treatment some silanols were removed by condensation between neighboring groups (Fig. 16 (d)), but their number was superior to those on the parent Y zeolite (Fig. 16 (a)).

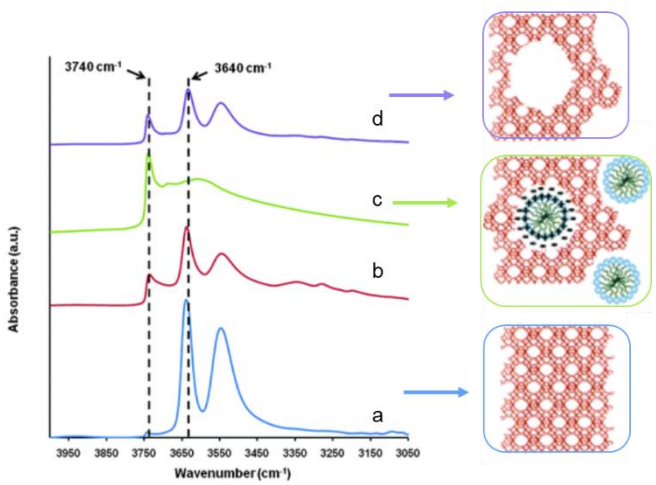

Fig. 16 *Infrared spectra of Y zeolites treated with NaOH and recrystallized in the presence of CTAB: (a) parent zeolite, (b) after dealumination with citric acid, (c) after treatment with CTAB and NaOH and (d) after calcination and NH_4^+ exchange. Effect of hot water treatment on silanol formation in zeolites. This figure has been adapted from ref 104 with permission from Royal Society of Chemistry, copyright 2012.*

3.3. Creation of defects by water intrusion

Water intrusion at high pressures also created defects in zeolites.[105,106] The method was applied on a defect-free silicalite-1 synthesized in fluoride media.[106] Isolated silanols, external silanols and silanol nests were created in the pure hydrophobic zeolite after the first water intrusion cycle. The mechanism to create such silanols by breaking siloxane bridges is highlighted in Fig. 17. The silanol defects created in a defect free silicalite-1 (fluoride synthesis) modified by high pressure water intrusion were however lower than observed on a synthesis in alkaline media.[106]

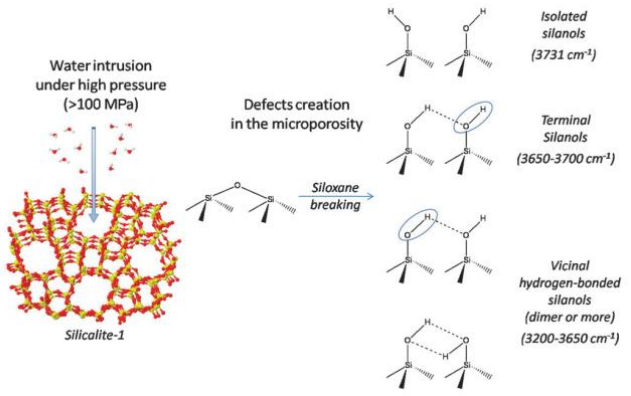

Fig. 17 *Silanol formation in highly hydrophobic silicalite-1 synthesized in fluoride media during water intrusion. This figure has been reproduced from ref 106 with permission from Royal Society of Chemistry, copyright 2010.*

A high pressure water intrusion post-synthesis treatment was also reported for the ITQ-7 structure.[107] A significant loss of water in the temperature range of 450-650 °C was observed by TG on a sample after a high pressure water intrusion cycle, attributed to silanols dehydroxylation formed during water intrusion.[107] The silanols were originated from siloxane breaking, Fig. 17. This was further supported by ^{29}Si NMR showing the emergence of a Q^3 peak and a decreased Q^4 peak resolution after the water intrusion. After a subsequent calcination, the Q^3 signal disappeared and the Q^4 resolution was improved, by annealing of such silanols.[107] The creation of additional defects was also observed in the ITQ-4 zeolite after water intrusion.[108] ^{1}H NMR highlighted an increase of the 2.2 ppm peak on the zeolite subjected to water intrusion. This peak appeared in the window of isolated and geminal silanols. Molecular simulation indicated that neighboring silanols and silanol nests could be produced during water intrusion in the ITQ-4 zeolite.[109]

3.4. Formation of defects by reduction of crystals size

As the layered materials described above, small zeolite crystals, whatever their preparation route, should contain such defects, as their external surface area becomes important. A linear correlation between the external surface of aggregated nanocrystals and the amount of external silanols (IR spectroscopy) was obtained as highlighted in

Fig. 18 *Linear correlation between external silanols (IR spectroscopy) and external surface area obtained (N_2 physisorption.*[110]

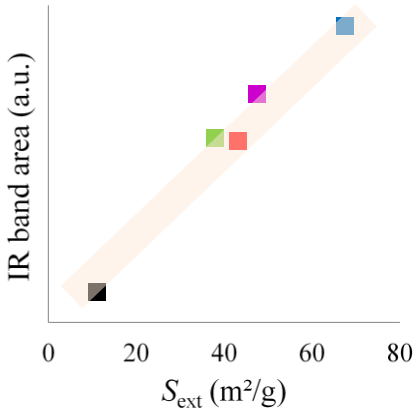

Fig. 18 *Linear correlation between external silanols (IR spectroscopy) and external surface area obtained (N_2 physisorption. This figure has been reproduced from ref 110 with permission from Elsevier, copyright 2019.*

The silica sources used for the synthesis of ZSM-5 played an important role on the resulting crystals with variable particle sizes.[111] Fumed silica generated cubic 55 nm crystals, while tetraethyl orthosilicate (TEOS) and colloidal silica produced 100 nm intergrowths. Although the above zeolite crystals were all in the micrometer range, the small crystallites observed may be an indication that the silica source could be responsible, in part at least, for the presence of silanols. [111–113]
A mixture of silicon sources (50% tetraethyl orthosilicate (TEOS) and 50% colloidal silica) in the preparation of silicalite-1 membranes yielded a higher degree of intergrowth and less thick self-supported layers.[113]
Impurities in the silica sources, such as Al, Fe, Ca and Mg, affected the synthesis of NaX zeolite as in their presence, crystal size decreased from 100 µm to about 20 µm.[114] Such a decrease in crystal size was associated with the presence of Al impurities around 200 ppm in silica source and only a few dozen ppm for other impurities.
The combined use of organic and inorganic structure directing agents in the synthesis of ZSM-5 was also studied.[115] For instance, a combination of cetyl trimethyl ammonium bromide (CTAB) and tetrapropylammonium bromide (TPABr) with different alkali metal hydroxides affected crystal size and morphology; the source of silica seemed again to play an important role. The crystals synthesized with tetraethyl orthosilicate (TEOS) were three times greater than those with colloidal silica (Ludox AS-30). The CTAB-Na combination appeared the most effective to produce small crystals. The alkali cations concentration in the synthesis was also reported to favor the formation of silanol nests in pure silica MFI zeolite (silicalite-1).[5]
The crystallization of an alkali metal (Na^+, K^+, Rb^+) chlorides gel leading to faujasite was also shown to play a role on the crystal sizes, i.e. the defects concentration.[116] Other methodologies generating nanocrystals are also available.[117–120] Some used metal-amine complexes as co-templates,[121] or a precise control of synthesis parameters such as time, temperature, gel composition and addition of seeds.[122,123] Reviews on the synthesis of nanozeolites are already available.[124–126]
The silanization of protozeolitic units to synthesize zeolites with controlled hydrophilicity was developed and extensively studied by Serrano and colleagues.[127,128] They used silanization agents to cover the surface of nano-nuclei formed in the initial stages of a hydrothermal synthesis and prevented these protozeolitic units to grow. Subsequent crystallization occurred around the silanization and intracrystalline mesopores appeared after removal of the organic templates by calcination. The usual structural defects were formed during this last step.
Growth modifiers were also used in zeolite synthesis to regulate crystal size. Such molecules selectively bind to a specific crystal face and modify its growth. For instance, Polyethylenimine (PEIM) generated 133 nm SSZ-13 crystals, much smaller than a conventional synthesis.[129] On the other hand, Poly (diallyldimethylammonium chloride) (PDDAC) addition in the synthesis of SSZ-13 increased crystal size to 23 µm, against 2.4 µm for crystals obtained through a conventional synthesis methodology. A combination of both PEIM and PDDAC yielded zeolites with tunable characteristics.[129]

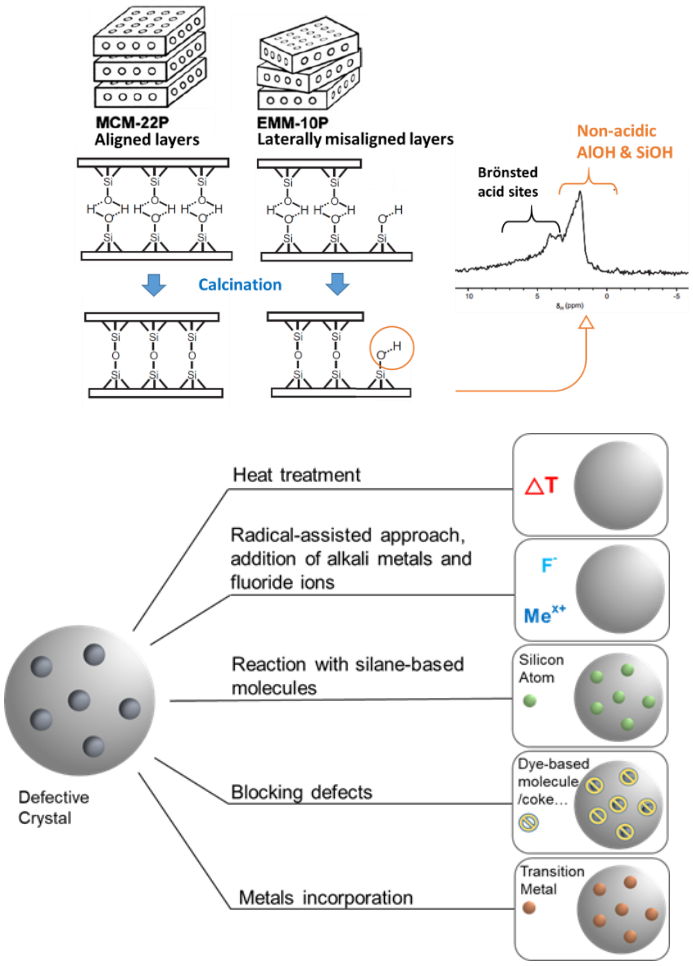

4. Healing defects in zeolites

Several techniques are available to heal the defects generated in zeolites. Some of the most promising and recurring methodologies on defect healing will be addressed below, as summarized in

Fig. ***19***.

Fig. 19 *Overview of strategies employed to heal zeolite defects.*

4.1. Heat treatment

Heat treatment (calcination) healed silanols and also induce structural changes in zeolitic materials. The calcination of a MWW precursor (PMCM-22) generated the 3D zeolite (MCM-22) by topotactic condensation of silanols at the zeolitic layers terminations.[130] Their microporous features were maintained and an independent pore system was formed by creation of 12 MR super-cavities.[131]

EMM-10P is another MWW layered structure precursor, but has a more disordered configuration of misaligned MWW layers.[132] The EMP-10 3D zeolite was obtained by the calcination of the precursor, and ^{1}H NMR indicated the presence of silanols, in addition to BAS (Fig. 20). The amount of silanols was higher (0.73 mole/g) than on the MCM-22 zeolite (0.46 mmol/g),[133] not presenting layer misalignment. Another example of silanols condensation upon calcination of layered precursors was the transformation of CIT-10 in the RTH structure upon calcination.[134] Other known zeolites, FER,[135] SOD,[136] and MTF[137] were also derived from layered precursors.

Fig. 20 *Schematic representation of the calcination of the layered precursors MCM-22P and EMM-10P and their silanols condensation. On the right, the ^{1}H MAS NMR spectrum of calcined EMM-10 zeolite is presented, with enhanced contribution of silanols due to layers misalignment. This figure has been adapted from ref 132 with permission from Elsevier, copyright 2011.*

The effect of calcination (heat treatment) on the healing of silanols nests in faujasite zeolite was investigated using infrared spectroscopy.[138] By increasing the treatment temperature, a progressive condensation of silanol nests was followed by IR. When the temperature reached 600 °C, the silanol nests were completely healed, while the external silanols were not affected. External silanols were probably isolated, avoiding then condensation with neighboring silanols. IR spectroscopy was also used by Bordiga et al.[139] to investigate the effect of calcination temperature on silanols in a silicalite-1. They observed that the condensation of silanols begins preferentially in those groups with stronger hydrogen bonds, as schematically presented in Fig. 21(a). With the increase in temperature (500°C), the formation of new peaks between 950 and 850 cm^{-1} in the IR spectra was attributed to the appearance of doubly bridged structures, formed by the condensation of vicinal silanol, as shown in Fig. 21 (b).[139]

Forni et al.[140] followed the evolution of silanols (terminal and H-bonded such as nests and bridging) as a function of calcination temperature on high silica MFI zeolites of different crystal sizes (2.5-70 µm) by {^{1}H} CP ^{29}Si NMR. The effect of pH during cation exchange to form H-MFI form was investigated as well. No clear trend between crystal size and silanols distribution appeared, but calcination at 450 °C and ion exchange in a basic medium, favored a higher concentration of H-bonded silanols.[140]

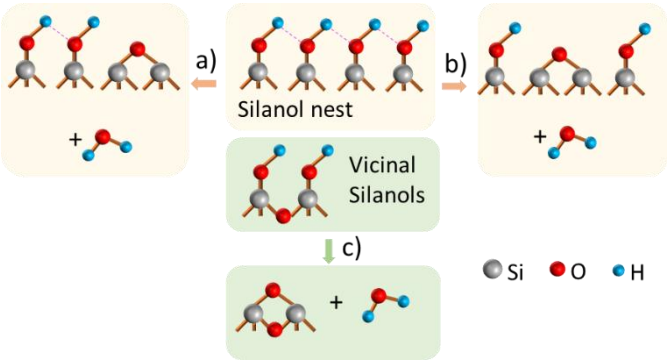

Fig. 21 *(a) A model for silanol condensation creating Si-O-Si bridges and (b) isolated silanols is presented. (c) a model representing the doubly bridged structure formation.*

In addition to calcination, other direct and post synthesis treatments can also heal defects.[85,141,142] Steam showed to be effective to cure silicalite-1 defects.[141] Furthermore, by varying the time of treatment, it was possible to control the extent of the defect healing.[141] The temperature of crystallization during the synthesis of zeolites also seemed to affect the amount of defects produced. In the case of ZSM-5 zeolite, a structure rich in defects could be obtained under hydrothermal synthesis at 100 °C. However, for an equivalent crystallization time, if the temperature was raised to 160 °C, the defects were cured.[85] Following the same pattern, the silicalite-1 crystallized at 180 °C presented a reduced amount of defects compared to a synthesis performed at 150 °C.[141,143]

4.2. Radical-assisted approach, addition of alkali metals and fluoride ions

Recently, hydroxyl radicals (OH*) showed their potential to heal zeolite defects.[144,145] OH* radicals, introduced during synthesis by chemical and physical methods, accelerated zeolite crystallization and favored the formation of high Si/Al zeolites by promoting the polymerization of silicate species. The OH* radical-assisted route also repaired silanol defects by the Si-O-Si condensation.

Alkaline cations combined with calcination was also a relevant procedure to heal defects. By raising the amount of Na^{+} it was possible to improve defect annealing during calcination, as shown from better resolved NMR spectra.[5] Furthermore, the calcination of samples containing F^{-} ions resulted in well resolved spectra, even better when compared to the scenario where alkali metals were present.[5,146] This result suggested that the F^{-} is a better defect healer than the alkali metals. The presence of F^{-} in the synthesis gel had already been explored widely and always resulted in zeolites with no or rare connectivity defects.[147–150] The effect of the F^{-} ions was even more striking when compared to the preparation of the same zeolite in OH^{-} medium.[150] The presence of F^{-} ions in the reaction medium allowed the total neutrality (or almost) of the positive charge introduced by the organic structure directing agents, which drastically reduced the formation of Si-O^{-} and therefore Si-OH.[149,150] Most of the time, F^{-} ions were

introduced into the synthesis through the use of HF as a mineralizing agent, but a recent study also points out the efficiency of other fluoride sources in reducing defects in zeolites.[151] The addition of ammonium fluoride (NH_4F) to a synthesis gel employing tetrapropylammonium hydroxide (TPAOH) as organic directing agent was reported to be responsible for reducing silanol nests in ZSM-5 zeolite. The reduction of silanol nests seemed to decrease with the increase in the F/Si ratios of zeolites.[151] Some post-treatments proposing the use of F- ions were also very straightforward for healing of silanol nest defects.[152–154] Promising results were obtained upon the post-treatment of defective zeolites with an aqueous mixture of NH_4F and tetraethylammonium hydroxide.[154] Elimination of silanol nest defects and high thermal stability of the treated zeolites were achieved. The treatment was very effective in the case of high silica zeolites, while the low silica zeolites presented thermal stability similar to the parent zeolites. According to the proposed mechanism of defect healing (
Fig. ***22***), silicon atoms migrated from some zone of the crystals in order to heal silanol nests. The silicon migration was then responsible for the formation of internal voids in the structure. Besides, tetraethylammonium hydroxide molecule was found to play an important role in the stabilization of the zeolitic structure during the treatment, as it acted as a pore filling agent.

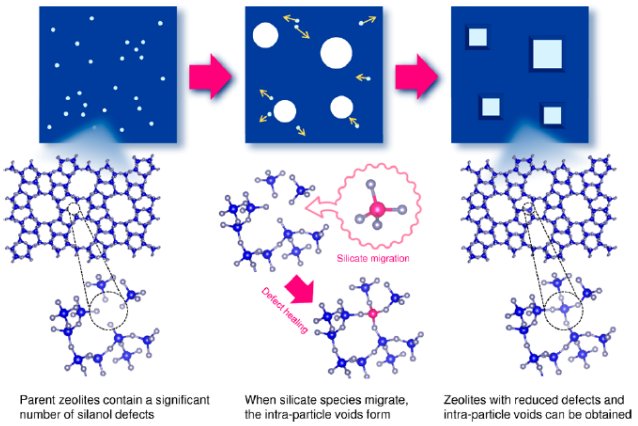

Fig. 22 *Proposed mechanism for the healing of defects in zeolites and concomitant formation of intraparticle voids. This figure has been reproduced from ref 154 with permission from American Chemical Society, copyright 2020.*

4.3. Reaction with silane-based molecules

A study carried out on pure silica MFI showed that in addition to silylation, the use of a basic pH during ion exchange process contributed to the reduction of defects.[155] Several defects in a zeolite BEA were healed by means of a silylation process using trimethylchlorosilane (TMS) agent.[156] The transformations occurred during the treatment with the silane molecule are schematized in Fig. 23 (a). Initially, the silane molecule interacted with the zeolite silanol groups, through condensation and subsequent HCl was released, forming a type of structure that was called "Sprimary". Next, the loss of the organic molecules (TMS) was observed through successive CH_4 releases. The elimination of the methyl groups from the trimethylchlorosilane molecule allowed the formation of other Si-O-Si bonds involving the Si initially present in the TMS and the Si in close silanol defects. These two factors combined were therefore responsible for the formation of the so called "Secondary" and "Sterciary" structures until the complete heal of a nest-like defect was achieved. The $\{^1H\}CP\ ^{29}Si$ NMR spectra (Fig. 23 (b)) indicated that even at low quantities of silane molecule, a significant reduction in Q_2 and Q_3 silanol groups was observed. It was also important to note that for new Si-O-Si bonds to be formed, the silanols originally present in zeolite had to be in close proximity and favored orientation. Otherwise, as for isolated silanols in the external surface, the creation of Si-O-Si bridges with other silanols was not possible.[156] These findings indicated that in this case, the silylation was more efficient for silanol nests. In addition, the accumulation of intermediate structures, such as those presented in Fig. 23, due to interactions with the silane molecule, could cause a decrease in the pore volume of the zeolite.

Fig. 23 *(a) Step-by-step representation of the process of silanol nest healing in BEA zeolite by means of sylilation with trimethylchlorosilane (TMS). The chemical shifts where each structure is observed are indicated, as well as the losses of molecules taking place in each step; (b) $\{^1H\}CP\ ^{29}Si$ NMR spectra of BEA zeolite before (defect form) and after sylilation (less defects) with different quantities of TMS. This figure has been reproduced from ref 156 with permission from American Chemical Society, copyright 2016.*

A functionalization with methyltrimethoxysilane was used for the production of spin-on zeolite films for application in microelectronics.[157,158] These films must have a hydrophobic character necessary to ensure good electrical performance. To do so, the methyltrimethoxysilane molecules were inserted in the reaction medium so that the Si-OH groups originated from the utilization of tetraethyl orthosilicate (TEOS) alone are replaced by $Si\text{-}CH_3$, which presents hydrophobic character.[157,158]

4.4. Blocking defects

The blocking of defects in an SSZ-13 zeolite membrane was promoted through a post treatment with a dye-based molecule (fluorescein sodium salt).[159] Such molecule presents an ideal size that allowed to access the defects, and at the same time prevented their entry into the zeolite pores. In this way, the defects were selectively blocked, without producing side effects such as compromising functional porosity of the zeolite. Furthermore, increasing the amount of dye-based molecule in the post-treatment solution favored the cure of a greater amount of defects.[159] Defects in zeolite membrane were also blocked by coking, promoting the connection between Si atoms in the defect walls, which were originally linked to OHs (silanols).[160] More specifically, silanols in the defects were expected to react with iso-propanol, creating $Si\text{-}O\text{-}C_3H_7$ groups through dehydration. Posteriorly, the defects were plugged by means of mild coking, forming Si-O-R, as represented in

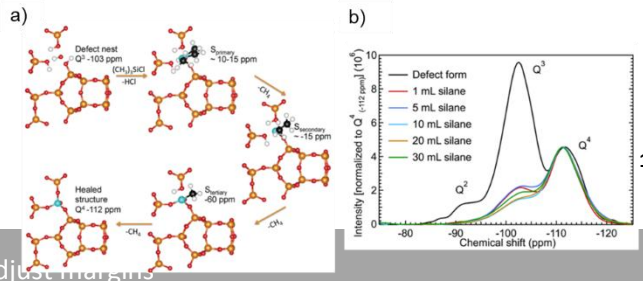

Fig. ***24***. The coking reaction for the blocking of defects proved to be highly efficient. Moreover, at least 90% of the zeolite pores were preserved by applying such method.[160]

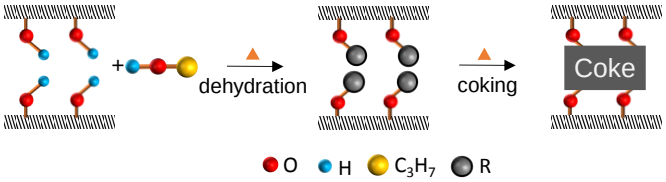

Fig. 24 *Defect blocking mechanism promoted by coking in zeolite membranes.*

4.5. Metals incorporation

Another strategy that has been considered to cure silanol defects in zeolites was based on the incorporation of different heteroatoms within the defect sites. Taramasso et al. were the first to accomplish the isomorphous substitution of Si with Ti in the Silicalite-1 (MFI) framework, and this led to the discovery of Titanium-Silicalite-1 (TS-1) used as oxidation catalyst.[161] The incorporation of heteroatoms in the zeolite framework was extended to other elements e.g. Ga, V and B.[162] The role of silanols in the incorporation of such elements was emphasized by using a dealuminated zeolite containing silanol groups that were found to react with vanadium complexes and allowed the incorporation of high amounts of V atoms.[163]

The use of a W precursor (sodium tungstate, Na_2WO_4) in the one-pot synthesis of MFI type zeolite was able to promote the formation of defect-free zeolite crystals.[164] Comparing the zeolite products synthesized in the absence and presence of heteroatoms (W, V, Mo, etc.), it was found that the metals occupied the defective silanol sites. The IR analysis indicated that silanol nests and isolated silanols were present in the as-made Si-MFI, while the presence of both was suppressed in the as-made tungsten containing zeolite (W-MFI). Another confirmation of silanol healing through the insertion of W was provided through ^{29}Si NMR analysis (Fig. 25). The zeolite resulting from the synthesis employing W did not present silanols (Q_2 and Q_3) and displayed highly resolved Q_4 signal, which was indicative of few defects. Accordingly, $\{^1H\}CP$ ^{29}Si NMR analysis did not indicate the presence of Q_3 or Q_2 silanols in W-MFI.[164] A direct synthesis applying Mo in the precursor suspensions was also shown to be effective in healing defects of MFI zeolite. For comparison pure silica MFI zeolite synthesized in fluoride media was added (sample F-MFI, spectra in green, Fig. 25). The Mo was reported to be inserted in the structure mainly occupying defective sites like silanol nests.[165] Likewise, T-vacant silanol groups in ZSM-5 obtained through dealumination were healed by the subsequent inclusion of Ti in the structure, which seemed to occupy such positions.[99] It was also shown that the use of an appropriate quantity of tin (IV) chloride pentahydrate during the synthesis of MFI nanosheets promoted the integration of Sn in tetrahedral coordination.[166] However, the hydrophilic character was still present in Sn-MFI nanosheets, due to the presence of silanols at the termination of the nanosheets. Considering the information above, one can suggest that metals have a preference in occupying vacant sites, such as silanol nests. As a result, a less effective cure of external isolated silanols was observed in comparison to silanol nests.

Recently, the healing of defects in an Al containing zeolite, more specifically ZSM-5, was accomplished through a hydrothermal post-synthesis treatment using sodium molybdate (Na_2MoO_4). Defects healing through hydrothermal treatment with Mo was compared to Mo impregnation in ZSM-5 zeolite. ^{29}Si NMR analyzes indicated that defects in ZSM-5 zeolite were healed thanks to the isomorphic substitution of Mo (during hydrothermal post-treatment), while through simple Mo impregnation the zeolite presented lots of defects. Furthermore, due to the cure of defects, the ZMS-5 zeolite containing Mo in the framework displayed excellent stability after catalytic tests and hydrothermal treatment.[167]

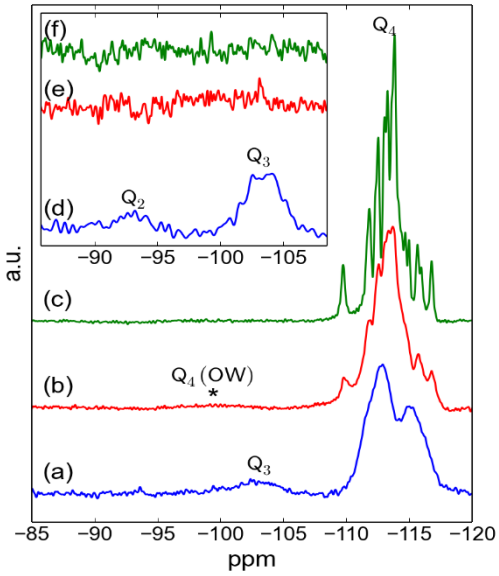

Fig. 25 *^{29}Si NMR spectra of as-synthesized Si-MFI (a), as-synthesized W-MFI (b), calcined F-MFI (c) zeolites. Inset: the $\{^1H\}CP$ ^{29}Si NMR spectra of Si-MFI (blue) and W-MFI (red) and F-MFI (green).*

Alkali metals certainly played an important role in the introduction of other metals in zeolites. Some of the works presented here considered the use of precursors containing sodium as Na_2WO_4 and Na_2MoO_4.[164,165,167] Furthermore, the influence of potassium, as an impurity incorporated through the use of organic template tetrapropylammonium hidroxide (TPAOH) source, was explored by Corma in the synthesis of Pt-MFI.[168] Interestingly, the amount of silanols in nests (~ 3500 cm^{-1}) was nonexistent in the sample containing traces of potassium (K-Pt-MFI), while a considerable amount of such silanos was observed in potassium-free zeolite (Pt-MFI). Furthermore, the authors mentioned that the silanol groups in the presence of K^+ would actually be transformed into -O-K^+ species, which facilitated interactions with Pt cations and favored the formation of -O-Pt species.

Throughout the last two sections, the methods affecting the defects in zeolites have been presented. The main methods addressed earlier to engineer and heal of defects in zeolites are summarized in

Table **3**.

Table 3 Methods used for engineering and healing of defects in zeolites

Engineering defects in zeolites		
Method	***Comments***	***Zeolite***
Synthesis of layered structures	Layered zeolites and materials derived from these structures through pillarization, delamination and others present large amounts of silanols. Nanosheets synthesized with amphiphilic surfactant and via intergrowth contain great amount of silanols.	MWW[67,68,70,72–75], MFI[76–79], FAU[80–82]
Generation of mesopores	The creation of mesopores in zeolite associated with the use of organic molecules favored the propagation of defects in the structure. Removing of organic molecules resulted in the formation of mesopores and induced silanols on the surface of the mesopores. Demetalation through acidic and basic treatments and steaming used in the production of mesopores created defects.	MFI[83–85,90–94,97–99,101–103],MOR[86–88], FAU [100,104]
Water intrusion	The intrusion of water at high pressures effectively broke siloxane bridges and created silanols in zeolites.	MFI[106], ISV[107], IFR[108,109]
Reduction of crystals size	Reducing the size of the zeolite crystals increased the amount of silanols at the termination of the crystals.	MFI[111,113,115,117–120], FAU[114,116], CHA[129], EDI[121], EMT[122], BEA[123]
Healing defects in zeolites		
Method	***Comments***	***Zeolite***
Heat treatment	Calcination promoted the condensation of silanols through topotactic condensation in layered zeolites. Vicinal silanols or H-bonded silanols in nests could also be cured by calcination or steam treatment, while isolated silanols seemed resistant to heat treatments. The high temperature hydrothermal treatment reduced silanol defects.	MFI[5,85,139–141,143]MWW[130–133], RTH[134], FER[135], SOD[136], MTF[137],FAU[138]
Alkali metals and F^- ions addition	The addition of alkali metals and F- ions in the synthesis precursor mixtures showed satisfactory effects in the reduction of silanols. Post-treatments using NH_4F were also promising in reducing defect sites.	MFI[5,146,148,151–154], ISV[147], CFI[150] BEA[154], MOR[153,154]
Silane-based molecules addition	The use of silane-based molecules directly in the synthesis gel or even for post-synthesis silylation proved to be effective in reducing silanols.	MFI[155], BEA [156], $MFI_{(low\text{-}k\ film)}$[157,158]
Blocking of defects	Silanol defects could be blocked through the use of dye-based molecules. The selective production of mild coke in silanols also promoted the disappearance of silanols.	CHA[159], MFI [160]

Metals incorporation	The insertion of transition metals in zeolite framework occurred especially in sites containing silanols. The cure of silanol nests justified the isomorphic substitution of metals.	MFI[99,164–168]

5. Impact of defects on zeolite applications: challenges and opportunities

As defects can be created, controlled and removed, they clearly belong to the toolbox of "Zeolite Crystal Engineering" to design materials fit for purpose in a wide variety of applications. The examples discussed in the following paragraph highlight the advantages and disadvantages of zeolite defects in catalysis, separation and biomedical applications.

As zeolitic silanols a have weak or moderate acidity, they can contribute to some reactions, e.g. selectivity, where strong acid sites are not required or even detrimental. The hydrophilicity of zeolitic silanols is also an asset in some reactions. Of course, the presence of silanols brings also problems as they tend to trap heavy hydrocarbons ("coke") leading to catalyst deactivation and severe regeneration conditions when coke is trapped inside the microporosity.

Silanol nests in silicalite-1 displayed a positive impact on both conversion and selectivity in the Beckmann rearrangement of cyclohexanone oxime to ε-caprolactam.[169] Increasing the concentration of silanol nests in HZSM-5 resulted in a more homogeneous distribution of ZnSnPt metal particles deposited by impregnation.[170] In addition, an appropriate distribution of the ZnSnPt Lewis sites, located in these silanol nests, was reported to favor the improvement in propane dehydrogenation.[170] In a recent theoretical work, the silanols groups in a SBA-15 material were identified as the activation sites in the reaction of acetone to enol-acetone.[171] In the production of propene from propan-2-ol on Silicalite-1, silanol nests were the only possible active sites converting up to 60% of the alcohol. Such a high conversion in the absence of aluminum was attributed to the presence of Brønsted sites in silicalite-1. The reaction scheme is outlined in Fig. 26.[172]

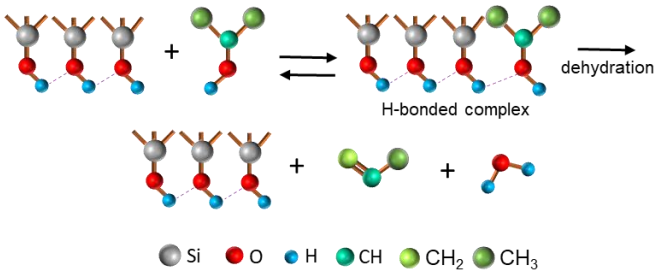

Fig. 26 *Schematic representation of the H-bonded silanol complexes and its role on the conversion of propan-2-ol.*

This may imply that different types of silanols (e.g., H-bonded as in nests and isolated silanols on the external surface) would display different catalytic activities. The Beckmann rearrangement of labeled ^{15}N-cyclohexanone oxime to ^{15}N-ε-caprolactam was evaluated on a defective silicalite-1 by means of ^{15}N NMR showing that silanol defects were active sites for this reaction.[173] Moreover, by comparing the activity of silicalite-1 by using ^{15}N-cyclohexanone oxime (free access to internal sites) and ^{15}N-cyclododecanone oxime (bulk and cannot access internal sites) as reagents, it was noticed that the internal H-bonded silanols were more active and more selective compared to external silanols.[173] Studies have also indicated that external silanols belonging to crystalline structures have an acidic character more important than the silanols in amorphous silica.[174] An enhanced acidity was observed in the first case where silanols present in ferrierite and ZSM-5 zeolite were able to react with C8-olefins as proton donors, contrary to silanols in amorphous silica that presented inert behavior under similar temperature(~-55°C). Such difference in the activity observed for the silanols in the different materials was certainly caused by the tension in the configuration of silanol groups when these were part of crystalline structures, as ferrierite and ZSM-5. On the contrary, silanols in the amorphous silica were described as occupying their most stable configuration, being thus less reactive. [174]

Some results also pointed to a synergistic effect between silanols in the vicinity of other active sites. The silanol nests present in a defective silicalite-1 were found to provide acidity for ethylenediamine (EDA) conversion, meanwhile this acidity could not ensure alone a high conversion.[175,176] In the case of the MFI zeolite containing Ti (TS-1), silanol groups in the vicinity of Ti sites were pointed as the ones responsible by the EDA condensation, rather than the Lewis acid sites from Ti(V). The higher acidity of silanols in TS-1 compared to silicalite-1 was related to an electronic effect or structural deformation generated by the Ti atom, as in

Fig. ***27***(a). The latter was responsible for reducing the strength of the neighboring SiO-H bond, which led to an easier release of the proton and thus enhanced acidity.[176]

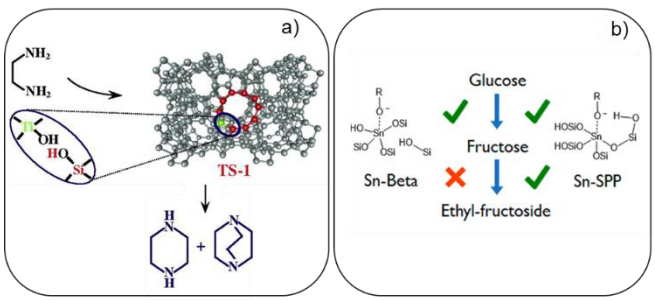

Fig. 27 *Silanol defects adjacent to (a) Ti sites in TS-1 zeolite and (b) Sn sites in Sn-Spp and its implication on ethylenediamine condensation and fructose etherification, respectively. Figure*

27 (a) has been reproduced from ref 176 with permission from Elsevier, copyright 2009. Figure 27 (b) has been reproduced from ref 177 with permission from American Chemical Society, copyright 2018.

A Sn-SPP catalyst, consisting of silanol rich MFI nanosheets, was active in both glucose isomerization and fructose etherification. On the other hand, a Sn-BEA with fewer defects did not catalyze the second reaction. According to theoretical studies, the presence of silanols in the vicinity of the Sn sites in the Sn-SPP could be responsible for the stabilization of the intermediate product, enabling fructose etherification (

Fig. ***27***(b)). Since silanols in Sn-BEA were more spaced and distant from the active sites, the reaction was not favored.[177]

In several applications, the hydrophilicity provided by silanols is a critical parameter. A high density of internal silanols was found to decrease the rate of glucose isomerization on Ti-Beta and Sn-Beta zeolites. The slower rate constants observed were explained by differences in transition state stability. Due to their hydrophilic character, silanols present in the zeolites were able to stabilize a network of water molecules. This water promoted the solvation of transition states, which hindered degrees of freedom, resulting in entropic penalties.[178,179] On the other hand, the stabilization of water networks on silanol nests had an opposite effect in the alkenes epoxidation reaction.[180] In the presence of silanol defects (zeolite with hydrophilic structure), the rate and selectivity of epoxidation increased compared to a defect-free zeolite. An entropic gain was favored by the epoxidation transition states, as they disrupted hydrogen bonds between water clusters and stabilizing silanol groups.[180]

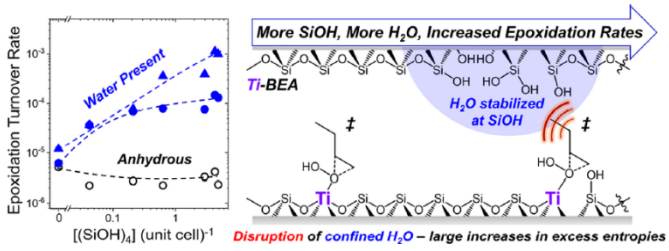

Fig. 28 *Representation of water clusters stabilized by silanol groups and the entropic gain caused by the disruption of the silanol-water interaction, due to the formation of epoxidation transition states. This figure has been reproduced from ref 180 with permission from American Chemical Society, copyright 2019.*

The hydrophilic character of Sn-MFI nanosheets was pointed as a possible parameter hindering its activity in the Baeyer-Villiger oxidation of cyclic ketones.[166] When the humidity was decreased during the reaction, a better performance of the catalyst was observed in terms of efficiency and number of moles converted per tin sites per hour. In an attempt to eliminate the silanols and thus the hydrophilic nature of the catalyst, the surface of the nanosheets was then silylated with triethoxymethylsilane. However, the silylation process was found to block the active sites. This study revealed the importance of understanding defects in zeolitic structures, as well as the search for alternative passivation methods toward controlling the defects sites.

The supplementary acidity generated by silanols is often considered as responsible for the formation of coke and deactivation of catalysts. *In-situ* IR study allowed to draw a correlation where the formation of coke during xylene isomerization led to a consumption of the bands related to silanol groups.[181,182] The presence of silanol defects in the ZSM-5 zeolite used in the synthesis of trioxane (TOX) from formaldehyde was the cause for the low selectivity and faster deactivation of the zeolite catalyst, compared to a catalyst with fewer defects.[151] In addition, selectivity for TOX was increased as the amount of silanol groups decreased. The amount of coke was also lower in the zeolites containing lower amount of silanols.[151]

The comparison of two zeolites, the sigma-1 and ZSM-58, in the conversion of methanol to olefin allowed to identify the effect of silanol defects.[183] Both zeolites displayed similar morphology and acidity, but sigma-1 had larger amounts of defects, which were scarce in ZSM-58 zeolite. The presence of silanol nests in sigma-1 proved to be responsible for the rapid formation of coke and deactivation of the catalyst, thus indicating the consequences that defects can trigger in catalysis. In addition, a moderate desilication treatment performed in the presence of NaOH and CTAB was reported to be efficient in the removal of silanol nest defects in sigma-1. This treatment promoted an increase in the lifetime of the sigma-1, easy recovery and catalytic performance close to the ZSM-58.[183]

Comparable studies on methanol to hydrocarbons conversion carried out using a ZSM-5 zeolite synthesized in both fluoride and basic medium indicated a similar conclusion where the presence of defects was responsible for a faster deactivation of the catalyst.[184,185] The presence of internal silanols in the zeolite synthesized in basic medium were found to be responsible for a more accelerated deactivation of the catalyst. UV-Raman analysis provided evidence that the deactivation of the sample synthesized in basic medium was related to the formation of molecular coke, deposited in the internal defects of the structure. The presence of coke in the internal microporosity hindered reagents diffusion, which contributed to a reduction of the catalyst performance.[185] The presence of mesopores, which facilitated the diffusion of coke precursor molecules, was found to reduce the deposition of coke in the structure of ZSM-5 during n-heptane aromatization.[186] The creation of mesopores combined with silanol defects healing proved to be very effective in reducing the catalyst deactivation rate.[186] Although the remarkable effect of mesopores, the annealing of silanols was reported to be even more effective in reducing the formation of coke. Such findings confirmed that coke precursor molecules were also formed in the internal silanols.[186]

Silicalite-1 films, derived from two different synthesis in fluoride and basic media with different amounts of defects, was tested for butanol adsorption.[187] An enhanced adsorption

capacity was observed for zeolite synthesized in basic medium, due to the possibility of butanol adsorption in silanol defect sites or even interaction through hydrogen bonds with water molecules, previously adsorbed in these silanols. On the other hand, a tenfold superior butanol/water selectivity was observed for the sample synthesized in a fluoride medium, due to the smaller amount of silanol defects.[187]

Defect annealing in ZSM-5 zeolite favored an increase in hexane adsorption capacity, in addition to a slight decrease in methane self-diffusion coefficient.[142] Furthermore, an enhanced mobility of adsorbed benzene in ZSM-5 zeolite with high density of defects was observed, certainly due to the greater flexibility of the structure afforded by the presence of defects. On the other hand, water adsorption capacity was significantly superior in the defective zeolite, but self-diffusion coefficient doubled after the defects were healed. Both behaviors observed for water adsorption and diffusion were related to the strong interaction of water molecules with the silanols defects.[142]

The adsorption of C2-C4 polyols was also found to increase with the amount of defects in silicalite-1. More specifically, propylene glycol adsorption was enhanced by a factor of 20 for silicalite-1 with the highest amount of defects (8.5 Si-OH/u.c.), compared to a defect-free silicalite-1.[141] A high adsorption capacity was also observed when investigating CO_2 adsorption in defective ZSM-58 and silicalite-1 zeolites.[188] With respect to ZSM-58, an increase in CO_2 adsorption linked to the presence of silanols was justified by the fact that such defects provided better access to smaller cavities in the structure. Regarding silicalite-1, the CO_2 adsorption capacity was higher for samples containing larger amounts of silanols. However, the adsorption gain was not proportional to the amount of silanols, which reinforces the hypothesis that CO_2 was not necessarily adsorbed in these silanols, but it was rather a consequence of the extra space created by the defects present in the structure.[188]

The blockage of the structural defects by water molecules was advantageous for CO_2 separation using defective SSZ-13 zeolite membrane under wet conditions[159,189] The healing of such defects resulted in a significant improvement of CO_2/N_2 and CO_2/CH_4 separation under dry conditions.[159] The reduction of internal and external defects in silicalite-1 also seemed to improve the selectivity in butanol/water separation.[190] Although tests in binary mixture water/butanol were not performed, the adsorption tests carried out individually for water and butanol indicated highest affinity for the latter.[190]

The interaction between silanols and adsorbate molecules was also investigated in the case of adsorption of Methyl tert-Butyl Ether (MTBE) on a high silica faujasite zeolite. The study indicated that hydrogen bonds were formed between the isolated external and internal silanols and the MTBE molecules, while the interaction with silanol nests were negligible. In addition, interactions with isolated silanols were found to result in the highest retention strength between the zeolite and the adsorbate.[191]

The interference of the defects goes beyond the issues with selectivity and they are also related to the creation of diffusion barriers. The interaction between surface silanols and adsorbates such as methane was shown to be an important limiter of the diffusion of molecules, causing diffusion barriers at the level of the surface of the crystals. Studies also point out that this resistance effect should be more important for small crystals, with a greater proportion of external surface silanols.[192]

The presence of silanols, among other characteristics, makes zeolites suitable for use in drug release applications based on their sorption behavior. The silanol groups in zeolites were used to make the connection between the surface of the zeolites and the drug through hydrogen bonds.[193] The presence of silanol groups on the surface of hierarchical zeolites, as well as ordered mesoporous materials, proved to be important in reducing the kinetics of drug release.[194] A study pointed out that the stronger the interactions between the silanol groups present on the surface of the material and the drug, the more promising the material was.[194] The presence of silanol defects in zeolites was also straightforward for other biomedical applications as cancer treatment, since these silanols were the key for the interaction between zeolite surface and cancer cells.[195] Furthermore, thanks to this characteristic of silanols, allowing adherence with cells, zeolite membranes have been successfully used as a support for cell growth.[196] The silanol groups also allowed the functionalization of the zeolite surface with groups that guaranteed a good interaction with bacteria cells. This type of functionalization improved the bactericidal activity on Ag^+ exchanged Y zeolite.[197] The application of zeolites in the medical field has also been extended to the study of bone implants. ZSM-5/hydroxyapatite composites were used as support for the growth of hydroxyapatite itself, which was used as bone implant. Silanol groups in the zeolite were responsible for the formation of an apatite layer, which promoted the formation of a bond between the implant and the bone.[198,199] Following the same trend, the presence of high amounts of silanols on the surface of the ZSM-5 nanozeolite in Ag-ZSM-5 matrix was pointed out as responsible for an accentuated formation hydroxyapatite.[200]

The effect of silanol defects on zeolite performance in catalysis, sorption and medical applications reported are summarized in Table 4.

Table 4 Effect of silanol defects in zeolites on catalysis and adsorption processes

Zeolites	Application	Comments	Reference
Catalysis			
Silicalite-1	Beckmann rearrangement of cyclohexanone oxime to ε-Caprolactam	Internal H-bonded silanols were more active and selective than external silanols.	[169,173]
Silicalite-1	Conversion of propan-2-ol to propylene	Silanol nests (Brønsted sites) increased conversion.	[172]
Silicalite-1 ZSM-5	Methane dehydroaromatization (MDA)	Healing of silanol defects provided ultra-stable single site metallic catalyst with improved stability and low coke production.	[164,165,167]
ZSM-5 BETA	Xylene isomerization	Silanols were responsible for coking and deactivation of catalysts.	[181,182]
ZSM-5	Synthesis of trioxane (TOX) from formaldehyde	Silanols caused low selectivity and faster deactivation.	[151]
ZSM-5	n-heptane aromatization	Creation of mesopores combined with healing of silanols reduced catalyst deactivation.	[186]
ZSM-5	Conversion of methanol to hydrocarbons	Defects responsible for fast deactivation due to coke deposited on internal defects.	[184,185]
TS-1, Sn-MFI Silicalite-1	Ethylenediamine (EDA) conversion	A synergy between silanols in the vicinity of Ti active sites was observed.	[175,176]
ZnSnPt-HZSM-5	Propane dehydrogenation (PDH)	Silanol nests promoted homogeneous distribution of metals.	[170]
Sn-BEA, Sn-SPP	Glucose isomerization and fructose etherification	Silanols in the vicinity of Sn responsible for stabilization of intermediate product and fructose etherification.	[177]
Sn-BEA	Sugar isomerization	High internal silanol defects decreased rate of sugar isomerization.	[178]
Ti-BEA	Alkenes epoxidation reaction	Stabilization of water networks over silanol nests enhanced rate of epoxidation and selectivity.	[180]
Sn-MFI	Baeyer-Villiger oxidation reaction	Terminal silanols hindered activity.	[166]
Sigma-1, ZSM-58	Methanol to olefin	Silanol nests responsible for	[183]

		rapid coke formation and deactivation.	
SBA-15	Acetone to enol-acetone	Silanos were active sites in the reaction of acetone to enol-acetone.	[171]
Adsorption and separation			
Silicalite-1	C2-C4 polyols adsorption	Adsorption enhanced with increasing defects.	[141]
Silicalite-1	Butanol adsorption Butanol/Water separation	Enhanced adsorption capacity and decreased butanol/water selectivity due to silanols. Reduction of internal and external defects improved selectivity in butanol/water separation.	[187,190]
Si-LTA	Methane adsorption	Surface silanols as diffusion barrier for methane.	[192]
ZSM-5	Hexane adsorption	Low defects content increased adsorption and decreased methane self-diffusion coefficient.	[142]
ZSM-58 Silicalite-1	CO_2 adsorption	High sorption capacity in the presence of silanol defects. Defects provided better access and extra space in the structure.	[188]
SSZ-13	CO_2/N_2 and CO_2/CH_4 separation	Healing structural defects by water improved CO_2/N_2 and CO_2/CH_4 separation.	[159,189]
High silica FAU	Methyl tert-Butyl Ether (MTBE) adsorption	Isolated silanols provided high retention strength for MTBE, while silanol nests had negligible effect.	[191]
ZSM-5/ Beta	Drug delivery	Kinetics of drug release reduced by silanols.	[193,194]
ZSM-5/hydroxyapatite	Biomedical application	Silanols improved interactions between zeolite surface and cancer cells. Silanols improved implants and bones interactions.	[195,196,198–200]
FAU with Ag+	Anti-bactericidal application	Silanols improved anti-bactericidal activity.	[197]

The main advantages and disadvantages of silanols in zeolites are schematically presented in **Erreur ! Source du renvoi introuvable.**. The presence of silanols can boost zeolite catalytic and adsorption efficiency while being very important in biomedical applications. However, silanols can also trigger some issues as coking, stability loss and low selectivity. In our group, the metal healing technique was developed, allowing healing the silanol defects at the same time a metallic site were introduced in the structure.[164,165,167] Therefore, silanol defects also contribute to a gain in versatility of zeolites, since they enable the insertion of different T-atoms in the zeolitic framework. Furthermore, the metal healing also allowed the production of zeolites with high stability and with low tendency for coke production, which overcomes the limitations of the presence of defects in zeolites.[167]

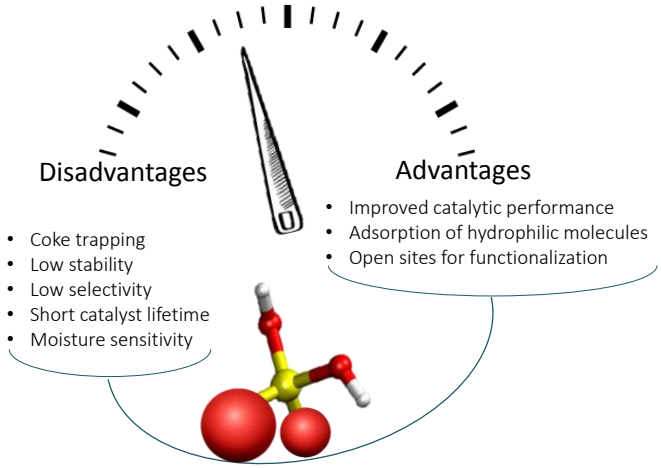

Fig. 29 Summary of the main advantages and disadvantages of silanol defects in zeolites.

6. Conclusions and outlook

The exact mechanism of formation and healing of zeolite defects is not yet established, but they are required to compensate unbalanced charges in the zeolitic structure. A defect-free network in pure silica would be almost useless in many applications. Introduction of Al^{+3}, or any T^{+3} cations in framework position, generates some of the most useful properties in zeolites: i) in catalysis bridged hydroxyls ([Si-O(H)-Al]) are BAS catalyzing a myriad of industrially relevant reactions ii) any other cation in the ([Si-O(X)-Al] (X= Na^{+}, K^{+}, ½ Mg^{++}, ½ Ca^{++}, ⅓ La^{+++}, ⅓Ce^{+++}…) leads to other catalytic applications, and selective adsorption. Other defects with lower acidity are located at crystal edges, on external surfaces, or in microporosity. Silanols (Si-OH) are observed at crystal terminations, while connectivity defects (geminal, vicinal, bridged and cluster types) occur when one or more T-O-T bonds are missing in the zeolite framework structures.

The main techniques used to characterize defects in zeolites are X-ray diffraction, UV-Vis, FTIR and NMR and DFT. The best strategy to describe zeolite defects is their combination as each one highlights a specific feature such as dynamics, atomic, and structural. Emerging and powerful new TEM methodologies are now available to locate hydrogen atoms and their further development will most probably add rich information on the structure of isolated or clustered hydrogen groups.[201]

While hierarchical zeolites, albeit used already in their first industrial applications in the early 60's, have been studied extensively in the last decade to promote faster molecular traffic in zeolites by lowering diffusion limitations, and the concomitant production of defects has not yet received the attention as it deserves.

We presented several direct synthesis approaches and post-synthesis treatments to create defects (layered zeolites, reduction of crystal size, creation of mesopores) and highlighted the associated generation of defects. Their presence is either beneficial or detrimental in catalysis for instance. Different methodologies to heal such defects are presented. In some cases, as in metal healing, defects act as ports of entry for novel isomorphous substitution (Mo, W, V…) producing new active sites in zeolites.

Defects in zeolites need further exploration, explanation and exploitation as they belong to the "Zeolite Crystal Engineering" toolbox to design the new catalysts and adsorbents required in the energy transition and in applications in emerging fields (biomedical, sensors, nanotechnology).

Abbreviations

Zeolite codes and material type	
BEA	Beta
CHA	Chabazite
CFI	California Institute of Technology – five
CIT-10	California Institute of Technology – ten
EDI	Edingtonite
EMT	Elf (or Ecole Supérieure) Mulhouse Chimie - two
FAU	Faujasite
FER	Ferrierite
IFR	Instituto de Tecnologia Quimica Valencia - four
ISV	Instituto de Tecnologia Quimica Valencia - seven
ITQ-2	Instituto de Tecnologia Quimica Valencia - two
ITQ-4	Instituto de Tecnologia Quimica Valencia - four
MWW	Mobil Composition of Matter-twenty-two
MCM-22	Mobil Composition of Matter –twenty-two
MCM-36	Mobil Composition of Matter – thirty-six
MCM-49	Mobil Composition of Matter – forty-nine
MCM-56	Mobil Composition of Matter – fifty-six
MEL	Zeolite Socony Mobil - eleven
MFI	Zeolite Mobil five
MIT-1	Massachusetts Institute of Technology - one
MOR	Mordenite
MTF	Mobil Composition of Matter - thirty-five
MTW	Zeolite Socony Mobil - twelve
RTH	Ruhr University Bochum - thirteen
SBA-15	Santa Barbara Amorphous-15
silicalite-1	Pure silica zeolite whose framework type is MFI
SOD	Sodalite
SPP	Self-Pillared Pentasil
SSZ-13	Standard Oil Synthetic Zeolite - thirteen
TON	Theta-1 (one)
TS-1	Titanosilicate whose framework type is MFI
X	X zeolite, whose framework type is faujasite (Si/Al~1-1.5)
Y (USY)	Y and ultrastable Y zeolite, whose framework type is faujasite (Si/Al>1.5)
ZSM-5	Zeolite Socony Mobil- five
ZSM-58	Zeolite Socony Mobil- fifty-eight
Chemical formulas	
CH_4	Methane
CO_2	Carbon dioxide
N_2	Nitrogen
NaOH	Sodium hidroxide
Na_2MoO_4	Sodium molybdate
Na_2WO_4	Sodium tungstate
NH_3	Ammonia
NH_4F	Ammonium fluoride
Characterization techniques	
DFT	Density Functional Theory
FTIR	Fourier Transform Infrared
HREM	High-Resolution Episcopic Microscopy
IR	Infrared
NMR	Nuclear Magnetic Resonance
TGA	Thermal Gravimetric Analysis
UV-Vis	Ultraviolet – Visible
XRD	X-Ray Diffraction

Others	
BAS	Brønsted acid sites
CTAB	Cetyl trimethyl ammonium bromide
C22	Polyquaternary ammonium surfactant
EDA	Ethylenediamine
EFAl	Extra framework aluminum
MTBE	Methyl tert-butyl ether
OSDA	Organic structure directing agent
PAM	Polyacrylamide
PDDAC	Poly-diallyldimethylammonium chloride
PEIM	Polyethylenimine
Si-OH	Silanol
[Si-O(H)-Al]	Brønsted acid sites
TBPO	Tributylphosphine oxide
TEOS	Tetraethyl orthosilicate
TMS	Trimethylchlorosilane
T-O-T	Bond between oxygen and two atoms in tetrahedron position
TOX	Trioxane
TPABr /TPAOH	Tetrapropylammonium bromide/ tetrapropylammonium hydroxide

Author Contributions

All authors contributed to this paper. ICMC and ED contributed equaly to the writing and design of figures.

Conflicts of interest

There are no conflicts to declare.

Acknowledgements

This research was supported by TOTAL and the Industrial Chair ANR-TOTAL “NanoClean Energy”.

References

1 E. M. Flanigen, in *Studies in Surface Science and Catalysis*, ed. J. C. J. H. van Bekkum, E.M. Flanigen, P.A. Jacobs, Elsevier Science B.V., 137th edn., 2001, pp. 11–35.

2 C. B. Lynne B. McCusker, in *Studies in Surface Science and Catalysis*, ed. A. C. iří Čejka, Herman van Bekkum, Elsevier, 2007, pp. 13–37.

3 M. Boronat and A. Corma, *Catal. Letters*, 2015, **145**, 162–172.

4 K. Hadjiivanov, *Identification and Characterization of Surface Hydroxyl Groups by Infrared Spectroscopy*, Elsevier Inc., 1st edn., 2014, vol. 57.

5 J. M. Chezeau, L. Delmotte, J. L. Guth and Z. Gabelica, *Zeolites*, 1991, **11**, 598–606.

6 G. Brunklaus, H. Koller and S. I. Zones, *Angew. Chemie*, 2016, **55**, 1–6.

7 C. Schroeder, C. Mück-lichtenfeld, L. Xu, N. A. Grosso-, A. Okrut, C. Chen, S. I. Zones, A. Katz, M. Ryan and H. Koller, *Angew. Chem. Int. Ed.*, 2020, **59**, 10939 –10943.

8 H. G. Karge, M. Hunger and H. K. Beyer, in *Catalysis and Zeolites*, Springer Berlin Heidelberg, 1999, pp. 198–326.

9 B. T. W. Lo, L. Ye and S. C. E. Tsang, *Chem*, 2018, **4**, 1778–1808.

10 T. B. Reed and D. W. Breck, *J. Am. Chem. Soc.*, 1956, **78**, 5972–5977.

11 W. M. Meier, *Zeitschrift fur Krist. - New Cryst. Struct.*, 1961, **115**, 439–450.

12 D. H. Olson and E. Dempsey, *J. Catal.*, 1969, **13**, 221–231.

13 H. van Koningsveld, H. van Bekkum and J. C. Jansen, *Acta Cryst.*, 1987, **B43**, 127–132.

14 C. Baerlocher, L. B. McCusker and D. H. Olson, *Atlas of Zeolite Framework Types, 6th Edition*, 2007.

15 J. Čejka, A. Corma and S. Zones, *Zeolites and Catalysis: Synthesis, Reactions and Applications*, Wiley-VCH Verlag GmbH & Co. KGaA, 2010, vol. 1–2.

16 S. J. L. B. Robert E. Dinnebier, *Powder Diffraction: Theory and Practice*, Royal Society of Chemistry, 2008.

17 L. B. McCusker and C. Baerlocher, *Zeitschrift fur Krist.*, 2013, **228**, 1–10.

18 Y. Yokomori and S. Idaka, *Microporous Mesoporous Mater.*, 1999, **28**, 405–413.

19 B. F. Mentzen, *J. Phys. Chem. C*, 2007, **111**, 18932–18941.

20 A. B. Pinar, L. Gómez-Hortigüela, L. B. McCusker and J. Pérez-Pariente, *Chem. Mater.*, 2013, **25**, 3654–3661.

21 B. T. W. Lo, L. Ye, J. Qu, J. Sun, J. Zheng, D. Kong, C. A. Murray, C. C. Tang and S. C. E. Tsang, *Angew. Chemie*, 2016, **128**, 6085–6088.

22 L. Ye, I. Teixeira, B. T. W. Lo, P. Zhao and S. C. E. Tsang, *Chem. Commun.*, 2017, **53**, 9725–9728.

23 C. Baerlocher, D. A. N. Xie, L. B. M. C. Cusker, S. Hwang, I. Y. Chan, K. Ong, A. W. Burton and S. I. Zones, *Nat. Mater.*, 2008, **7**, 631–635.

24 S. Smeets, Z. J. Berkson, D. Xie, S. I. Zones, W. Wan, X. Zou, M. F. Hsieh, B. F. Chmelka, L. B. McCusker and C. Baerlocher, *J. Am. Chem. Soc.*, 2017, **139**, 16803–16812.

25 S. Bordiga, C. Lamberti, F. Bonino, A. Travert and F. Thibault-Starzyk, *Chem. Soc. Rev.*, 2015, **44**, 7262–7341.

26 E. Brunner, H. Pfeifer and H. G. Karge, *Zeitschrift fur Phys.*

Chemie, 1992, **176**, 173–183.
27 A. Erigoni, S. H. Newland, G. Paul, L. Marchese, R. Raja and E. Gianotti, *ChemCatChem*, 2016, **8**, 3161–3169.
28 J. P. Gallas, J. M. Goupil, A. Vimont, J. C. Lavalley, B. Gil, J. P. Gilson and O. Miserque, *Langmuir*, 2009, **25**, 5825–5834.
29 D. D. Laws, H.-M. L. Bitter and A. Jerschow, *Angew. Chemie Int. Ed.*, 2002, **41**, 3096–3129.
30 H. Koller and M. Weiß, *Top. Curr. Chem.*, 2012, **306**, 189–228.
31 G. Engelhardt, *Trends Anal. Chem.*, 1989, **8**, 343–347.
32 E. Lippmaa, A. Samoson and M. Mägi, *J. Am. Chem. Soc.*, 1986, **108**, 1730–1735.
33 C. Fernandez and M. Pruski, *Top. Curr. Chem.*, 2012, **306**, 119–188.
34 J. J. Dědeček, S. Sklenak, C. Li, B. Wichterlová, V. Gábová, J. Brus, M. Sierka and J. Sauer, *J. Phys. Chem. C*, 2009, **113**, 1447–1458.
35 O. H. Han, C.-S. Kim and S. B. Hong, *Angew. Chemie Int. Ed.*, 2002, **41**, 469–472.
36 C. Schroeder, V. Siozios, M. Hunger, M. R. Hansen and H. Koller, *J. Phys. Chem. C*, 2020, **124**, 23380–23386.
37 C. Schroeder, V. Siozios, C. Mück-Lichtenfeld, M. Hunger, M. R. Hansen and H. Koller, *Chem. Mater.*, 2020, **32**, 1564–1574.
38 S. Xin, Q. Wang, J. Xu, Y. Chu, P. Wang, N. Feng, G. Qi, J. Trébosc, O. Lafon, W. Fan and F. Deng, *Chem. Sci.*, 2019, **10**, 10159–10169.
39 L. Peng, Y. Liu, N. Kim, J. E. Readman and C. P. Grey, *Nat. Mater.*, 2005, **4**, 216–219.
40 H. Huo, L. Peng, Z. Gan and C. P. Grey, *J. Am. Chem. Soc.*, 2012, **134**, 9708–9720.
41 G. P. M. Bignami, D. M. Dawson, V. R. Seymour, P. S. Wheatley, R. E. Morris and S. E. Ashbrook, *J. Am. Chem. Soc.*, 2017, **139**, 5140–5148.
42 S. M. Pugh, P. A. Wright, D. J. Law, N. Thompson and S. E. Ashbrook, *J. Am. Chem. Soc.*, 2020, **142**, 900–906.
43 F. A. Perras, U. Chaudhary, I. I. Slowing and M. Pruski, *J. Phys. Chem. C*, 2016, **120**, 11535–11544.
44 E. Dib, T. Mineva, P. Gaveau and B. Alonso, *Phys. Chem. Chem. Phys.*, 2013, **15**, 18349–18352.
45 E. Dib, T. Mineva, P. Gaveau, E. Véron, V. Sarou-Kanian, F. Fayon and B. Alonso, *J. Phys. Chem. C*, 2017, **121**, 15831–15841.
46 V. M. Mastikhin, I. L. Mudrakovsky and A. V. Nosov, *Prog. Nucl. Magn. Reson. Spectrosc.*, 1991, **23**, 259–299.
47 A. A. Gabrienko, I. G. Danilova, S. S. Arzumanov, L. V. Pirutko, D. Freude and A. G. Stepanov, *J. Phys. Chem. C*, 2018, **122**, 25386–25395.
48 E. Dib, J. Grand, S. Mintova and C. Fernandez, *Chem. Mater.*, 2015, **27**, 7577–7579.
49 E. Dib, J. Grand, A. Gedeon, S. Mintova and C. Fernandez, *Microporous Mesoporous Mater.*, 2021, **315**, 110899.
50 A. J. Vega and Z. Luz, *J. Phys. Chem.*, 2002, **91**, 365–373.
51 J. M. Kobe, T. J. Gluszak, J. A. Dumesic and T. W. Root, *J. Phys. Chem.*, 2002, **99**, 5485–5491.
52 T. J. Gluszak, D. T. Chen, S. B. Sharma, J. A. Dumesic and T. W. Root, *Chem. Phys. Lett.*, 1992, **190**, 36–41.
53 P. S. Sidhu, J. Bell, G. H. Penner and K. R. Jeffrey, *Can. J. Chem.*, 1996, **74**, 1784–1794.
54 J. Hunger, I. A. Beta, H. Böhlig, C. Ling, H. Jobic and B. Hunger, *J. Phys. Chem. B*, 2005, **110**, 342–353.
55 P. Błoński, A. Birczyński, Z. T. Lalowicz, J. Datka and Z. Łodziana, *J. Phys. Chem. C*, 2015, **119**, 19548–19557.
56 G. Li, X. Wang, X. Guo, S. Liu, Q. Zhao, X. Bao and X. Lin, *Mater. Chem. Phys.*, 2001, **71**, 195–201.
57 J. Dědeček and B. Wichterlová, *J. Phys. Chem. B*, 1999, **103**, 1462–1476.
58 J. Dědeček, Z. Sobalík and B. Wichterlová, *Catal. Rev. - Sci. Eng.*, 2012, 54, 135–223.
59 D. H. Brouwer, *J. Am. Chem. Soc.*, 2008, **130**, 6306–6307.
60 D. H. Brouwer and G. D. Enright, *J. Am. Chem. Soc.*, 2008, **130**, 3095–3105.
61 S. Cadars, D. H. Brouwer and B. F. Chmelka, *Phys. Chem. Chem. Phys.*, 2009, **11**, 1825–1837.
62 C. Martineau, S. Vial, D. Barth, F. Quessette and F. Taulelle, *Solid State Nucl. Magn. Reson.*, 2015, **65**, 84–88.
63 E. Dib, T. Mineva, E. Veron, V. Sarou-Kanian, F. Fayon and B. Alonso, *J. Phys. Chem. Lett.*, 2018, **9**, 19–24.
64 G. Sastre, V. Fornes and A. Corma, *J. Phys. Chem. B*, 2002, **106**, 701–708.
65 A. J. Jones and E. Iglesia, *ACS Catal.*, 2015, **5**, 5741–5755.
66 L. Treps, C. Demaret, D. Wisser, B. Harbuzaru, A. Méthivier, E. Guillon, D. V. Benedis, A. Gomez, T. De Bruin, M. Rivallan, L. Catita, A. Lesage and C. Chizallet, *J. Phys. Chem. C*, 2021, **125**, 2163–2181.
67 A. Corma, V. Fornes, S. B. Pergher, T. L. M. Maesen and J. G. Buglass, *Nature*, 1998, **396**, 353–356.
68 W. J. Roth, P. Nachtigall, R. E. Morris and C. Jir, *Chem. Rev.*, 2014, **114**, 4807−4837.
69 M. Tsapatsis, *AIChE J.*, 2014, **60**, 2374–2381.
70 W. J. Roth, C. T. Kresge, J. C. Vartuli, A. S. Lenowicz and A. S. Fung, *Catal. by Microporous Mater.*, 1995, **94**, 301–308.
71 Y. J. He, G. S. Nivarthy, F. Eder, K. Seshan and J. A. Lercher, *Microporous Mesoporous Mater.*, 1998, **25**, 207–224.
72 P. Wu, J. Ruan, L. Wang, L. Wu, Y. Wang, Y. Liu, W. Fan, M. He, O. Terasaki and T. Tatsumi, *J. Am. Chem. Soc.*, 2008, **130**, 8178–8187.
73 L. Jiang, Y. Gong, X. Meng, L. Zhang, Y. Zhai, L. Meng, M. Materials, Y. Gong, X. Meng, L. Zhang, Y. Zhai, S. Shang and L. Meng, *Microporous Mesoporous Mater.*, 2020, **302**, 110245.
74 S. L. Lawton, A. S. Fung, G. J. Kennedy, L. B. Alemany, C. D. Chang, G. H. Hatzikos, D. N. Lissy, M. K. Rubin, H.-K. C. Timken, S. Steuernagel and D. E. Woessner, *J. Phys. Chem.*, 1996, **100**, 3788–3798.
75 H. Y. Luo, V. K. Michaelis, S. Hodges, R. G. Griffin and Y. Roman-Leshkov, *Chem. Sci*, 2015, **6**, 6320–6324.
76 Y. Zhao, Z. Ye, H. Zhang, Y. Zhang and Y. Tang, *Ind. Eng. Chem. Res.*, 2019, **58**, 13174–13181.
77 L. Emdadi and D. Liu, *J. Mater. Chem. A*, 2014, **2**, 13388–13397.
78 D. Xu, G. R. Swindlehurst, H. Wu, D. H. Olson, X. Zhang and M. Tsapatsis, *Adv. Funct. Mater.*, 2014, **24**, 201–208.
79 M. Choi, K. Na, J. Kim, Y. Sakamoto, O. Terasaki and R.

Ryoo, *Nature*, 2009, **461**, 246–249.
80 A. Inayat, I. Knoke, E. Spiecker and W. Schwieger, *Angew. Chemie - Int. Ed.*, 2012, **51**, 1962–1965.
81 M. Khaleel, A. J. Wagner, K. A. Mkhoyan and M. Tsapatsis, *Angew. Chemie - Int. Ed.*, 2014, **53**, 9456–9461.
82 A. Inayat, C. Schneider and W. Schwieger, *Chem. Commun.*, 2015, **51**, 279–281.
83 M. Choi, H. S. Cho, R. Srivastava, C. Venkatesan, D. H. Choi and R. Ryoo, *Nat. Mater.*, 2006, **5**, 718–723.
84 D. H. Lee, M. Choi, B. W. Yu and R. Ryoo, *Chem. Commun.*, 2009, 74–76.
85 B. Peng, H. Zou, L. He, P. Wang, Z. Shi, L. Zhu, R. Wang and Z. Zhang, *CrystEngComm*, 2017, **19**, 7088–7094.
86 Y. Jin, Y. Li, S. Zhao, Z. Lv, Q. Wang, X. Liu and L. Wang, *Microporous Mesoporous Mater.*, 2012, **147**, 259–266.
87 S. G. Song, *Mater. Res.*, 1999, **14**, 2616–2620.
88 H. Sheng, W. Qian, H. Zhang, P. Zhao, H. Ma and W. Ying, *Microporous Mesoporous Mater.*, 2020, **295**, 1387–1811.
89 M. Hunger, D. Freude, H. Pfeifer and W. Schwieger, *Chem. Phys. Lett.*, 1990, **167**, 21–26.
90 J. C. Groen, G. M. Hamminga, J. A. Moulijn and J. Pérez-Ramírez, *Phys. Chem. Chem. Phys.*, 2007, **9**, 4822–4830.
91 J. C. Groen, L. A. A. Peffer, J. A. Moulijn and J. Pérez-Ramírez, *Stud. Surf. Sci. Catal.*, 2005, **156**, 401–408.
92 J. C. Groen, J. C. Jansen, J. A. Moulijn and J. Pérez-Ramírez, *J. Phys. Chem. B*, 2004, **108**, 13062–13065.
93 Q. Shen, M. Wu, H. Wang, N. Sun, C. He and W. Wei, *Appl. Surf. Sci.*, 2018, **441**, 474–481.
94 R. Qi, T. Fu, W. Wan and Z. Li, *Fuel Process. Technol.*, 2017, **155**, 191–199.
95 D. Verboekend, K. Thomas, M. Milina, S. Mitchell, J. Pérez-Ramírez and J.-P. Gilson, *Catal. Sci. Technol.*, 2011, **1**, 1331–1335.
96 D. Verboekend, M. Chabaneix, K. Thomas, J. Gilson and P. Javier, *CrystEngComm View*, 2011, **13**, 3408–3416.
97 P. J. Kooyman, P. van der Waal and H. van Bekkum, *Zeolites*, 1997, **18**, 50–53.
98 D. D. Anggoro, S. B. Sasongko, L. Buchori, K. C. Sulistyani, A. Oktavijaya and H. Oktavianty, *IOP Conf. Ser. Mater. Sci. Eng.*, 2019, **578**, 012027.
99 J. H. C. VAN Kraushaa, B.R.Hoof, *Catal. Letters*, 1988, **1**, 81–84.
100 C. McDaniel and P. Maher, in *Molecular Sievess, Soc. Chem. Ind.*, London, 1968, pp. 186–194.
101 L. H. Ong, M. Dömök, R. Olindo, A. C. Van Veen and J. A. Lercher, *Microporous Mesoporous Mater.*, 2012, **164**, 9–20.
102 M. Rostamizadeh and F. Yaripour, *J. Taiwan Inst. Chem. Eng.*, 2017, **71**, 454–463.
103 A. R. Maag, G. A. Tompsett, J. Tam, C. A. Ang, G. Azimi, A. D. Carl, X. Huang, L. J. Smith, R. L. Grimm, J. Q. Bond and M. T. Timko, *Phys. Chem. Chem. Phys.*, 2019, **21**, 17880–17892.
104 J. García-Martínez, M. Johnson, J. Valla, K. Li and J. Y. Ying, *Catal. Sci. Technol.*, 2012, **2**, 987–994.
105 G. Fraux, F. X. Coudert, A. Boutin and A. H. Fuchs, *Chem. Soc. Rev.*, 2017, **46**, 7421–7437.
106 T. Karbowiak, M. A. Saada, S. Rigolet, A. Ballandras, G. Weber, I. Bezverkhyy, M. Soulard, J. Patarin and J. P. Bellat, *Phys. Chem. Chem. Phys.*, 2010, **12**, 11454–11466.
107 L. Tzanis, B. Marler, H. Gies and J. Patarin, *J. Phys. Chem. C*, 2013, **117**, 4098–4103.
108 M. A. Saada, S. Rigolet, J. L. Paillaud, N. Bats, M. Soulard and J. Patarin, *J. Phys. Chem. C*, 2010, **114**, 11650–11658.
109 Y. G. Bushuev and G. Sastre, *J. Phys. Chem. C*, 2011, **115**, 21942–21953.
110 I. C. Medeiros-Costa, C. Laroche, J. Pérez-Pellitero and B. Coasne, *Microporous Mesoporous Mater.*, 2019, **287**, 167–176.
111 R. M. Mohamed, H. M. Aly, M. F. El-shahat and I. A. Ibrahim, *Microporous Mesoporous Mater.*, 2005, **79**, 7–12.
112 G. Song, W. Chen, P. Dang, Y. Wang and F. Li, *R. Soc. open sci.*, 2018, **5**, 181691.
113 P. Hrabanek, A. Zikanova, J. Drahokoupil, O. Prokopova, L. Brabec, I. Jirka, M. Matejkova, V. Fila, O. De Iglesia and M. Kocirik, *Microporous Mesoporous Mater.*, 2013, **174**, 154–162.
114 K. E. Hamilton, E. N. Coker, A. Sacco, A. G. Dixon and R. W. Thompson, *Zeolites*, 1993, **13**, 645–653.
115 A. Chawla, R. Li, R. Jain, R. J. Clark, J. G. Sutjianto, J. C. Palmer and J. D. Rimer, *Mol. Syst. Des. Eng.*, 2018, **3**, 159–170.
116 N. Dewaele, P. Bodart, Z. Gabelica and J. B. Nagy, *Stud. Surf. Sci. Catal.*, 1985, **24**, 119–128.
117 S. A. Pelster, W. Schrader and F. Schüth, *J. Am. Chem. Soc.*, 2006, **128**, 4310–4317.
118 C. E. A. Kirschhock, R. Ravishankar, L. Van Looveren, P. A. Jacobs and J. A. Martens, *J. Phys. Chem. B*, 1999, **103**, 4972–4978.
119 C. E. A. Kirschhock, R. Ravishankar, F. Verspeurt, P. J. Grobet, P. A. Jacobs and J. A. Martens, *J. Phys. Chem. B*, 1999, **103**, 4965–4971.
120 D. Lesthaeghe, P. Vansteenkiste, T. Verstraelen, A. Ghysels, C. E. A. Kirschhock, J. A. Martens, V. Van Speybroeck and M. Waroquier, *J. Phys. Chem. C*, 2008, **112**, 9186–9191.
121 N. Zeolites, M. Amine, U. M. R. Cnrs and A. Werner, *Chem. Mater.*, 2007, **19**, 1203–1205.
122 E. Ng, J. Goupil, C. Fernandez, R. Retoux, V. Valtchev and S. Mintova, *Chem. Mater.*, 2012, **24**, 4758–4765.
123 G. Majano, L. Delmotte, V. Valtchev and S. Mintova, *Chem. Mater.*, 2009, **21**, 4184–4191.
124 S. Mintova, J. P. Gilson and V. Valtchev, *Nanoscale*, 2013, **5**, 6693–6703.
125 L. Tosheva and V. P. Valtchev, *Chem. Mater.*, 2005, **17**, 2494–2513.
126 V. Valtchev and L. Tosheva, *Chem. Rev.*, 2012, **113**, 6734–6760.
127 D. P. Serrano, J. M. Escola and P. Pizarro, *Chem. Soc. Rev.*, 2013, **42**, 4004–4035.
128 D. P. Serrano, J. Aguado, J. M. Escola, A. Peral, G. Morales and E. Abella, *Catal. Today*, 2011, **168**, 86–95.
129 M. Kumar, H. Luo, Y. Roman-Leshkov and D. Rimer, *J. Am. Chem. Soc.*, 2015, **137**, 13007–13017.
130 US4954325, 1990.

131 S. L. Lawton, M. E. Leonowicz, R. D. Partridge, P. Chu and M. K. Rubin, *Microporous Mesoporous Mater.*, 1998, **23**, 109–117.

132 W. J. Roth, D. L. Dorset and G. J. Kennedy, *Microporous Mesoporous Mater.*, 2011, **142**, 168–177.

133 G. J. Kennedy, M. Afeworki, D. C. Calabro, C. E. Chase and R. J. Smiley, *Appl. Spectrosc.*, 2004, **58**, 698–704.

134 J. Schimidt, D. Xie and M. E. Davis, *Chem. Sci*, 2015, **6**, 5955–5963.

135 L. Schreyeck, P. Caullet, J. C. Mougenel, J. L. Guth and B. Marler, *Microporous Mater.*, 1996, **6**, 259–271.

136 T. Moteki, W. Chaikittisilp, A. Shimojima and T. Okubo, *J. Am. Chem. Soc.*, 2008, **130**, 15780–15781.

137 A. Rojas and M. a. Camblor, *Chem. Mater.*, 2014, **26**, 1161–1169.

138 T. Kawai and K. Tsutsumi, *J. Colloid Interface Sci.*, 1999, **212**, 310–316.

139 S. Bordiga, P. Ugliengo, A. Damin, C. Lamberti, G. Spoto, A. Zecchina, G. Spanò, R. Buzzoni and L. Dalloro, *Top. Catal.*, 2001, **15**, 43–52.

140 L. Forni, G. Fornasari, G. Giordano, C. Lucarelli, A. Katovic, F. Trifirò, C. Perri and J. B. Nagy, *Phys. Chem. Chem. Phys.*, 2004, **6**, 1842–1847.

141 E. E. Mallon, M. Y. Jeon, M. Navarro, A. Bhan and M. Tsapatsis, *Langmuir*, 2013, **29**, 6546–6555.

142 M. Hunger, J. Kärger, H. Pfeifer, J. Caro, B. Zibrowius, M. Bülow and R. Mostowicz, *J. Chem. Soc. Faraday Trans. 1 Phys. Chem. Condens. Phases*, 1987, **83**, 3459–3468.

143 H. Koller, R. F. Lobo, S. L. Burkett and M. E. Davis, *J. Phys. Chem*, 1995, **99**, 12588–12596.

144 D. Shi, L. Xu, P. Chen, T. Ma, C. Lin, X. Wang, D. Xu and J. Sun, *Chem. Commun.*, 2019, **55**, 1390–1393.

145 G. Feng, P. Cheng, W. Yan, M. Boronat, X. Li, J.-H. Su, J. Wang, Y. Li, A. Corma, R. Xu and J. Yu, *Science*, 2016, **351**, 1188 LP – 1191.

146 I. Grosskreuz, H. Gies and B. Marler, *Microporous Mesoporous Mater.*, 2020, **291**, 109683.

147 A. Corma and V. Forne, *Angew. Chemie Int. Ed.*, 2000, **39**, 2346–2349.

148 J. Patarin, M. Soulard, H. Kessler, J. L. Guth and J. Baron, *Zeolites*, 1989, **9**, 397–404.

149 P. Caullet, J. L. Paillaud, A. Simon-Masseron, M. Soulard and J. Patarin, *Comptes Rendus Chim.*, 2005, **8**, 245–266.

150 P. A. Barrett, M. J. Díaz-Cabañas, M. A. Camblor and R. H. Jones, *J. Chem. Soc. - Faraday Trans.*, 1998, **94**, 2475–2481.

151 Y. Ye, M. Yao, H. Chen and X. Zhang, *Catal. Letters*, 2020, **150**, 1445–1453.

152 Z. Qin, L. Lakiss, J. Gilson, K. Thomas, J. Goupil, C. Fernandez and V. Valtchev, *Chem. Mater.*, 2013, **25**, 2759–2766.

153 Z. Qin, G. Melinte, J.-P. Gilson, M. Jaber, K. Bozhilov, P. Boullay, S. Mintova, O. Ersen and V. Valtchev, *Angew. Chemie Int. Ed.*, 2016, **55**, 15049–15052.

154 K. Iyoki, K. Kikumasa, T. Onishi, Y. Yonezawa, A. Chokkalingam, Y. Yanaba, T. Matsumoto, R. Osuga, S. P. Elangovan, J. N. Kondo, A. Endo, T. Okubo and T. Wakihara, *J. Am. Chem. Soc.*, 2020, **142**, 3931-.

155 P. Lanzafame, K. Barbera, S. Perathoner, G. Centi, A. Aloise, M. Migliori, A. MacArio, J. B. Nagy and G. Giordano, *J. Catal.*, 2015, **330**, 558–568.

156 S. Prodinger, M. A. Derewinski, A. Vjunov, S. D. Burton, I. Arslan and J. A. Lercher, *J. Am. Chem. Soc.*, 2016, **138**, 4408–4415.

157 S. Li, Z. Li, D. Medina, C. Lew and Y. Yan, *Chem. Mater.*, 2005, **17**, 1851–1854.

158 S. Eslava, J. Urrutia, A. N. Busaworv, M. R. Baklanov, F. Iacopi, S. Aldea, K. Maex, J. A. Martens and C. E. A. Kirschhock, *J. Am. Chem. Soc.*, 2008, **130**, 17528–17536.

159 S. Hong, D. Kim, Y. Jeong, E. Kim, J. C. Jung, N. Choi, J. Nam, A. C. K. Yip and J. Choi, *Chem. Mater.*, 2018, **30**, 3346–3358.

160 D. Korelskiy, P. Ye, M. S. Nabavi and J. Hedlund, *J. Mater. Chem. A*, 2017, **5**, 7295–7299.

161 *United States Pat.*, 1983.

162 R. Millini, G. Perego and G. Bellussi, *Top. Catal.*, 1999, **9**, 13.

163 S. Dzwigaj, P. Massiani, A. Davidson and M. Che, *J. Mol. Catal. A Chem.*, 2000, **155**, 169–182.

164 J. Grand, S. N. Talapaneni, A. Vicente, C. Fernandez, E. Dib, H. A. Aleksandrov, G. N. Vayssilov, R. Retoux, P. Boullay, J. Gilson, V. Valtchev and S. Mintova, *Nature Materials*, 2017, **16**, 1010–1015.

165 F. Dubray, S. Moldovan, C. Kouvatas, J. Grand, C. Aquino, N. Barrier, J. Gilson, N. Nesterenko, D. Minoux and S. Mintova, *J. Am. Chem. Soc.*, 2019, **141**, 8689–8693.

166 H. Y. Luo, L. Bui, W. R. Gunther, E. Min and Y. Roma, *ACS Catal.*, 2012, **2**, 2695−2699.

167 S. V. Konnov, F. Dubray, E. B. Clatworthy, C. Kouvatas, J. Gilson, J. Dath, D. Minoux, C. Aquino, V. Valtchev, S. Moldovan, S. Koneti, N. Nesterenko and S. Mintova, *Angew. Chemie*, 2020, 19553– 19560.

168 L. Liu, M. Lopez-Haro, C. W. Lopes, C. Li, P. Concepcion, L. Simonelli, J. J. Calvino and A. Corma, *Nat. Mater.*, 2019, **18**, 866–873.

169 G. P. Heitmann, G. Dahlhoff and W. . Holderich, *J. Catal.*, 1999, **186**, 12–19.

170 W. Zhou, J. Liu, J. Wang, L. Lin, N. He, X. Zhang and H. Guo, *Catalysts*, 2019, **9**, 571.

171 J. Zhang, Z. Wang, Y. Lyu, H. Xie, T. Qi, Z. Si, L. Liu, H. Yang and C. Hu, *J. Phys. Chem. C*, 2019, **123**, 4903−4913.

172 E. Janiszewska, A. Macario, J. Wilk, A. Aloise, S. Kowalak, J. B. Nagy and G. Giordano, *Microporous Mesoporous Mater.*, 2013, **182**, 220–228.

173 A. B. Fernández, M. Boronat, T. Blasco and A. Corma, *J. Cat*, 2007, **249**, 116–119.

174 J. N. Kondo, E. Yoda, H. Ishikawa, F. Wakabayashi and K. Domen, *J. Catal.*, 2000, **281**, 275–281.

175 Y. Zhang, L. Lin, X. Zheng, C. Liu, Q. Zhu and H. Guo, *Catalysts*, 2020, **10**, 1–15.

176 Y. Wang, Y. Liu, X. Li, H. Wu, M. He and P. Wu, *J. Catal.*, 2009, **266**, 258–267.

177 T. R. Josephson, R. F. Dejaco, S. Pahari, L. Ren, Q. Guo, M. Tsapatsis, J. I. Siepmann, D. G. Vlachos and S. Caratzoulas, *ACS Catal.*, 2018, **8**, 9056–9065.

178 J. C. Vega-vila and R. Gounder, *ACS Catal.*, 2020, **10**, 12197–12211.

179 M. J. Cordon, J. W. Harris, J. Carlos Vega-Vila, J. S. Bates, S. Kaur, M. Gupta, M. E. Witzke, E. C. Wegener, J. T. Miller, D. W. Flaherty, D. D. Hibbitts and R. Gounder, *J. Am. Chem. Soc.*, 2018, **140**, 14244–14266.

180 D. T. Bregante, A. M. Johnson, A. Y. Patel, E. Z. Ayla, M. J. Cordon, B. C. Bukowski, R. Gounder and D. W. Flaherty, *J. Am. Chem. Soc.*, 2019, **141**, 7302–7319.

181 A. Vimont, O. Marie, J. P. Gilson, J. Saussey and J. C. Lavalley, *Stud. Surf. Sci. Catal.*, 1999, **126**, 147–154.

182 F. Thibault-starzyk, A. Vimont and J. Gilson, *Catal. Today*, 2001, **70**, 227–241.

183 I. Prokopyeva, J. Goetze, C. Gucuyener, L. Van Thiel, A. Dikhtiarenko, J. Ruiz-Martinez, B. Weckhuysen, J. Gascon and F. Kapteijn, *Catal. Sci. Technol.*, 2016, **6**, 2663–2678.

184 Z. Qin, L. Lakiss, L. Tosheva and J. Gilson, *Adv. Funct. Mater.*, 2014, **24**, 257–264.

185 M. Grahn, A. Faisal, O. G. W. Öhrman, M. Zhou, M. Signorile, V. Crocellà, M. Sadegh and J. Hedlund, *Catal. Today*, 2020, **345**, 136–146.

186 K. Lee, S. Lee, Y. Jun and M. Choi, *J. Catal.*, 2017, **347**, 222–230.

187 A. Farzaneh, R. F. Dejaco, L. Ohlin, A. Holmgren, J. I. Siepmann and M. Grahn, *Langmuir*, 2017, **33**, 8420−8427.

188 A. Vidoni, P. I. Ravikovitch, M. Afeworki, D. Calabro, H. Deckman and D. Ruthven, *Microporous Mesoporous Mater.*, 2019, **294**, 109818.

189 V. A. Online, N. Kosinov, J. Gascon, F. Kapteijn and E. J. M. Hensen, *Mater. Chem. A*, 2014, **2**, 13083–13092.

190 A. Farzaneh, M. Zhou, O. N. Antzutkin, J. Hedlund, A. Holmgren and M. Grahn, *Langmuir*, 2016, **32**, 11789–11798.

191 I. Braschi, G. Gatti, C. Bisio, G. Berlier, V. Sacchetto, M. Cossi and L. Marchese, *J. Phys. Chem. C*, 2012, **116**, 6943–6952.

192 A. F. Combariza and G. Sastre, *J. Phys. Chem. C*, 2011, **115**, 13751–13758.

193 Y. P. Guo, T. Long, Z. F. Song and Z. A. Zhu, *J. Biomed. Mater. Res. - Part B Appl. Biomater.*, 2014, **102**, 583–591.

194 R. A. García-Muñoz, V. Morales, M. Linares, P. E. González, R. Sanz and D. P. Serrano, *J. Mater. Chem. B*, 2014, **2**, 7996–8004.

195 P. Tavolaro, G. Martino, S. Andò and A. Tavolaro, *Mater. Sci. Eng. C*, 2016, **69**, 894–904.

196 P. Tavolaro, S. Catalano, G. Martino and A. Tavolaro, *Appl. Surf. Sci.*, 2016, **380**, 135–140.

197 S. A. M. Hanim, N. A. N. N. Malek and Z. Ibrahim, *Appl. Surf. Sci.*, 2016, **360**, 121–130.

198 N. Iqbal, M. R. A. Kadir, S. Iqbal, S. Izwan, A. Razak, M. S. Ra, H. R. Bakhsheshi-rad, M. Hasbullah, M. A. Khattak, H. R. B. Raghavendran and A. A. Abbas, *Ceram. Int.*, 2016, **42**, 1–8.

199 H. Takadama, H. Kim and T. Kokubo, *Chem. Mater.*, 2001, **1**, 1108–1113.

200 B. Kaur, R. Srivastava, B. Satpati, K. K. Kondepudi and M. Bishnoi, *Colloids Surfaces B Biointerfaces*, 2015, **135**, 201–208.

201 M. S. Palatinus L, Brázda P, Boullay P, Perez O, Klementová M, Petit S, Eigner V, Zaarour M, *Science,* 2017, **355**, 166–169.